HHS Public Access

Author manuscript

Sci Immunol. Author manuscript; available in PMC 2023 May 26.

Published in final edited form as:

Sci Immunol. 2023 March 17; 8(81): eabn7993. doi:10.1126/sciimmunol.abn7993.

An XBP1s–PIM-2 positive feedback loop controls IL-15–mediated survival of natural killer cells

Shoubao Ma[1,2,†], **Jingjing Han**[1,2,†], **Zhenlong Li**[1,2,†], **Sai Xiao**[1,2], **Jianying Zhang**[3], **Jiazhuo Yan**[1], **Tingting Tang**[1], **Tasha Barr**[1], **Andrew S. Kraft**[4], **Michael A. Caligiuri**[1,2,5,*], **Jianhua Yu**[1,2,5,6,*]

[1]Department of Hematology and Hematopoietic Cell Transplantation, City of Hope National Medical Center, Los Angeles, CA 91010, USA.

[2]Hematologic Malignancies Research Institute, City of Hope National Medical Center, Los Angeles, CA 91010, USA.

[3]Department of Computational and Quantitative Medicine, City of Hope National Medical Center, Los Angeles, CA 91010, USA.

[4]University of Arizona Cancer Center, University of Arizona, Tucson, AZ 85724, USA.

[5]Comprehensive Cancer Center, City of Hope, Los Angeles, CA 91010, USA.

[6]Department of Immuno-Oncology, Beckman Research Institute, City of Hope, Los Angeles, CA 91010, USA.

Abstract

Spliced X-box–binding protein 1 (XBP1s) is an essential transcription factor downstream of interleukin-15 (IL-15) and AKT signaling, which controls cell survival and effector functions of human natural killer (NK) cells. However, the precise mechanisms, especially the downstream targets of XBP1s, remain unknown. In this study, by using XBP1 conditional knockout mice, we found that XBP1s is critical for IL-15–mediated NK cell survival but not proliferation in vitro and in vivo. Mechanistically, XBP1s regulates homeostatic NK cell survival by targeting PIM-2, a critical anti-apoptotic gene, which in turn stabilizes XBP1s protein by phosphorylating it at Thr[58]. In addition, XBP1s enhances the effector functions and antitumor immunity of NK cells by recruiting T-bet to the promoter region of *Ifng*. Collectively, our findings identify a previously unknown mechanism by which IL-15–XBP1s signaling regulates the survival and effector functions of NK cells.

[*]Corresponding author. jiayu@coh.org (J. Yu); mcaligiuri@coh.org (M.A.C.).
[†]These authors contributed equally to this work.

Author contributions: S.M., J. Yu, and M.A.C. conceived and designed the project. S.M., J.H., Z.L., S.X., J. Yan, T.T., and J.Z. performed experiments and/or data analyses. A.S.K. provided the PIM-2 KO mice. S.M., T.B., J. Yu, and M.A.C. wrote, reviewed, and/or revised the paper. J. Yu and M.A.C. supervised the research and acquired funding. All authors discussed the results and commented on the manuscript.

Competing interests: The authors declare that they have no competing interests.

Data and materials availability: The RNA-seq and ChIP-seq data were deposited in the Gene Expression Omnibus (GSE188796 and GSE218543). All data needed to evaluate the conclusions in the paper are present in the paper or the Supplementary Materials.

INTRODUCTION

Natural killer (NK) cells are innate immune cells that directly eliminate tumor cells and virus-infected cells and elicit other adaptive immune responses (1, 2). Upon activation, they produce a distinct set of cytokines such as interferon-γ (IFN-γ), tumor necrosis factor–α (TNF-α), granzyme B, and perforin. NK cells also secrete chemokines such as C-C motif chemokine ligand 1 (CCL1), CCL2, CCL3, and CCL4. In immunotherapy, NK cells have emerged as safe and promising treatments for patients with certain cancers (3, 4). For example, chimeric antigen receptors (CARs) can be used to direct NK cells toward tumor cells carrying the corresponding antigens (5, 6). However, it remains challenging to enhance NK cell cytotoxicity and persistence in vivo in NK cell–directed therapies (4).

The endoplasmic reticulum (ER) is the main cellular compartment committed to protein folding and maturation within eukaryotes, which is critical for maintaining cell homeostasis (7). However, the accumulation of unfolded or misfolded proteins that are beyond ER protein-folding capacity may result in a stress condition termed “ER stress” (7). Cells will activate the unfolded protein response (UPR) to alleviate the unfolded protein load, which is controlled by three ER stress sensors: protein kinase RNA-like ER kinase (PERK) (8), inositol-requiring enzyme 1 (IRE1) (9), and activating transcription factor 6 (ATF6) (10). IRE1α is maintained in a repressed state under nonstress conditions through an association with ER chaperone-binding immunoglobulin protein (BiP). Upon ER stress, BiP dissociates and binds misfolded proteins, leading to partial IRE1α phosphorylation and dimerization (11). Activation of IRE1α triggers the splicing of X-box–binding protein 1 (XBP1) mRNA to produce an active transcriptional activator, spliced XBP1 (XBP1s) (12, 13). XBP1s regulates the transcriptional programs of UPR target genes encoding ER chaperones (*Hspa5, Ddit3, ERdj4, Pdia3*, and *Dnajc3*) (14), ER-associated protein degradation components (*Edem1, Herpud1*, and *Hrd1*) (15, 16), folding enzyme (*Pdia6*) (14), ER translocon (*Sec61a1*) (17), and other transcription factors (*Klf9* and *Foxo1*) (18, 19). The IRE1α-XBP1 signaling pathway is implicated in a wide range of biological processes, including tumorigenesis, lipid and glucose metabolism, immune cell development, and immune responses (17, 20-25).

Our group previously reported that XBP1s is an essential transcription factor downstream of interleukin-15 (IL-15) and AKT signaling that controls cell survival and effector functions in human NK cells (26). XBP1s also facilitates NK cell proliferation during mouse cytomegalovirus (MCMV) infection by regulating c-Myc (27), indicating that it plays a fundamental role in controlling NK cell immunity. However, the target genes downstream of XBP1s in NK cells have not been identified in the cytokine activation setting, nor is it known how XBP1s regulates NK cell survival and effector functions. Endogenous XBP1s has a short half-life because it is rapidly destroyed by proteasomes (28). We previously showed that, in human NK cells, AKT maintains XBP1s stability by inhibiting its ubiquitination and therefore degradation (26). It has also been reported that XBP1s is stabilized when it is phosphorylated by p38 mitogen-activated protein kinase (MAPK) and IκB kinase β (IKKβ) (28, 29). However, whether there are other factors that contribute to the stability of XBP1s in NK cells is unknown.

In this study, we used XBP1 conditional knockout (cKO) mice to explore how XBP1s regulates NK cell survival and effector functions. Our findings reveal that XBP1s is critical for IL-15–mediated NK cell survival. Mechanistically, XBP1s regulates NK cell survival by targeting PIM-2, a critical anti-apoptotic gene, in a positive feedback loop. Moreover, XBP1s enhances NK cells' effector functions and antitumor immunity by interacting with T-bet to promote IFN-γ production. Collectively, our findings uncover detailed mechanisms by which IL-15–XBP1s signaling controls the survival and effector functions of NK cells.

RESULTS

XBP1s is required for NK cell homeostasis under ER stress

To define the role of XBP1s in NK cell homeostasis in vivo, we generated NK cell–specific cKO mice by crossing *Xbp1*$^{f/f}$ mice (30) with *Ncr1*-iCre mice (31) (hereafter called *Xbp1*^{cKO} mice). *Xbp1*$^{f/f}$ mice were used as littermate controls. XBP1s deletion in NK cells was verified by quantitative polymerase chain reaction (qPCR) and immunoblotting (fig. S1A). Phenotypic analyses revealed that the frequencies and absolute numbers of NK cells were similar in the bone marrow (BM), spleen, and lung (fig. S1B) in *Xbp1*^{cKO} mice compared with *Xbp1*$^{f/f}$ mice, indicating that XBP1s does not affect NK cell homeostasis at steady state. In addition, XBP1s deficiency did not affect NK cell maturation, as shown by CD11b and CD27 staining (fig. S1C). These results are consistent with a prior study showing that XBP1 is dispensable for NK cell basal homeostasis (27).

We explored the role of XBP1 in NK cell homeostasis in different ER stress conditions including during ectopic IL-15 expression, a tumor challenge model, and an experimental autoimmune encephalomyelitis (EAE) model. We first treated mice with IL-15, as we previously did for human NK cells (26). The frequencies and absolute numbers of NK cells were significantly lower in *Xbp1*^{cKO} mice than in *Xbp1*$^{f/f}$ mice (Fig. 1A). To further explore the role of XBP1s in the presence of abundant IL-15 protein in vivo, we crossed *Xbp1*^{cKO} mice with our IL-15 transgenic (Tg) mice (32, 33) to generate *Il15*^{Tg}*Xbp1*^{cKO} mice (fig. S1D). *Il15*^{Tg}*Xbp1*^{cKO} mice showed a significantly reduced frequency and absolute number of NK cells compared with the *Il15*^{Tg}*Xbp1*$^{f/f}$ mice (Fig. 1B), similar to mice treated with IL-15. However, NK cell maturation did not change substantially in the mice treated with IL-15 or in the *Il15*^{Tg} mice (fig. S1, E and F).

Tumor microenvironment factors, such as hypoxia and nutrient deprivation, can activate ER stress and UPR responses (34). We found that *Xbp1*^{cKO} mice had significantly higher B16-F10 melanoma tumor colonies than *Xbp1*$^{f/f}$ mice (fig. S1G). Furthermore, the percentage and the absolute number of tumor-infiltrating NK cells were significantly lower in *Xbp1*^{cKO} mice compared with those in *Xbp1*$^{f/f}$ mice (Fig. 1C). We also performed experiments using the mouse EAE model to induce another ER stress condition (35, 36). *Xbp1*^{cKO} mice displayed a reduced EAE score compared with *Xbp1*$^{f/f}$ mice (fig. S1H). We found a significantly reduced percentage and absolute number of NK cells in the brains of *Xbp1*^{cKO} mice compared with those from *Xbp1*$^{f/f}$ mice at the onset of EAE (Fig. 1D). Together, these results indicate that XBP1s is required for NK cell homeostasis under conditions of stress defined by excessive IL-15, cancer, and autoimmunity.

XBP1s controls IL-15–mediated NK cell survival but not proliferation

To investigate the mechanism by which XBP1s signaling regulates NK cell homeostasis, we examined the proliferation and survival of XBP1-deficient NK cells at steady state and under the three aforementioned conditions. NK cells from *Xbp1*$^{f/f}$ and *Xbp1*^{cKO} mice had similar proliferation and survival at steady state, as evidenced by Ki67 staining and annexin V staining, respectively (fig. S2, A and B). IL-15–treated *Xbp1*^{cKO} mice and *Xbp1*$^{f/f}$ mice had comparable percentages of Ki67^{+} proliferating NK cells, as did*Il15*$^{Tg-}$ *Xbp1*^{cKO} mice compared with *Il15*^{Tg}*Xbp1*$^{f/f}$ mice (fig. S2, C and D). In addition, a 5-ethynyl-2′-deoxyuridine (EdU) incorporation assay further showed that NK cell proliferation rate was similar between *Xbp1*$^{f/f}$ and *Xbp1*^{cKO} mice in the BM, spleen, and liver (fig. S2, E to G). However, the viability of NK cells was significantly lower in the IL-15–treated *Xbp1*^{cKO} mice or *Il15*^{Tg}*Xbp1*^{cKO} mice than in the IL-15–treated *Xbp1*$^{f/f}$ or *Il15*^{Tg}*Xbp1*$^{f/f}$ mice, respectively, as evidenced by annexin V staining (Fig. 2, A and B). Similarly, decreased survival but unchanged proliferation was observed in NK cells from *Xbp1*^{cKO} mice compared with those from *Xbp1*$^{f/f}$ mice with tumor challenge or at the onset of EAE disease (fig. S2, H and I). These results suggest that the defects of NK cell homeostasis by XBP1s ablation at steady or tumor challenge states may be due to disrupted cell survival but not proliferation.

We then used the ectopic IL-15 model to further investigate the detailed mechanism by which XBP1s signaling controls NK cell survival. We isolated splenic NK cells from *Xbp1*^{cKO} mice and *Xbp1*$^{f/f}$ mice and cultured them in the presence of IL-15 in vitro. The NK cells from the *Xbp1*^{cKO} mice showed significantly less growth than those from the *Xbp1*$^{f/f}$ mice (Fig. 2C). NK cells from the *Xbp1*^{cKO} mice that were expanded in vitro with IL-15 also exhibited significantly more rapid cell death after IL-15 was withdrawn from the environment than those from the *Xbp1*$^{f/f}$ mice (Fig. 2D). A CellTrace Violet (CTV) labeling assay and a 5-bromo-2′-deoxyuridine (BrdU)/7-aminoactinomycin D (7-AAD) incorporation assay showed that both the proliferation and division of NK cells were unimpaired by XBP1 deficiency during IL-15 stimulation (fig. S2, J and K). However, NK cells from the *Xbp1*^{cKO} mice exhibited significantly more apoptosis than those from the *Xbp1*$^{f/f}$ mice, as evidenced by annexin V staining (Fig. 2E), active caspase-3 staining (Fig. 2F), and the fluorochrome-labeled inhibitors of caspases (FLICA) assay (Fig. 2G).

Activated NK cells undergo activation-induced cell death mediated by the Fas-FasL pathway (37, 38). NK cells also express TNF-related apoptosis-inducing ligand (TRAIL), which triggers cell death by receptor-mediated apoptosis (39). To investigate whether the NK cell survival defect mediated by XBP1s deficiency is caused by FasL or TRAIL-induced cell apoptosis, we analyzed the expression levels of FasL and TRAIL in NK cells from *Xbp1*$^{f/f}$ and *Xbp1*^{cKO} mice before and after stimulating with IL-15. We found that the expression levels of FasL and TRAIL were similar between NK cells from *Xbp1*$^{f/f}$ and those from *Xbp1*^{cKO} mice with or without IL-15 stimulation (fig. S3, A and B). Using neutralizing antibodies to block FasL or TRAIL could not reduce NK cell apoptosis mediated by XBP1 deficiency in response to IL-15 (fig. S3C). These results suggest that XBP1s-mediated NK cell survival is independent of FasL and TRAIL. Collectively, these murine studies demonstrate that XBP1s controls IL-15–mediated NK cell survival but not proliferation.

This conclusion is consistent with our prior finding that XBP1s positively regulates IL-15–mediated cell survival in human NK cells (26).

XBP1s maintains NK cell survival by targeting PIM-2 in mice

To identify the downstream target genes of XBP1s in NK cells, we performed RNA sequencing (RNA-seq) analysis in NK cells purified from the spleens of *Il15*^{Tg}*Xbp1*^{cKO} mice and *Il15*^{Tg}*Xbp1*$^{f/f}$ mice. We focused on splenic NK cells because NK cells isolated from the spleen had the highest expression levels of XBP1s when stimulated with IL-15 compared with NK cells from the BM, liver, and lung (fig. S4A). We also performed chromatin immunoprecipitation coupled with high-throughput DNA sequencing (ChIP-seq) in splenic NK cells purified from *Il15*^{Tg}*Xbp1*$^{f/f}$ mice. Two independent biological replicates were performed. Overlapping analysis using BEDTools (40) showed that 4890 peaks were present in both replicates (fig. S4B). The majority of the XBP1 binding peaks were enriched in the promoter regions (65.56%) and intergenic regions (21.35%) (fig. S4, C and D), indicating that it binds both promoters and potential enhancers. The search for enriched motifs using HOMER revealed a sequence element, 5′-CACGTCA-3′, as the highest score motif with $P = 1 \times 10^{-172}$, which is identical to the XBP1 binding motif defined from the JASPAR database and from mouse T helper 2 (T_H2) cells (fig. S4E). In addition, the Kyoto Encyclopedia of Genes and Genomes (KEGG) pathway enrichment analysis revealed that the peaks were mainly enriched in terms of “protein processing in endoplasmic reticulum,” “protein export,” “cell cycle,” and “apoptosis” (fig. S4F), which is consistent with the known biological role of XBP1. Consistent with a prior study in T_H2 cells, we also found strong binding peaks around the promoter of XBP1 itself in NK cells (fig. S4G), suggesting that XBP1 has autoregulation ability.

Gene Ontology analysis of RNA-seq data demonstrated that differentially expressed genes (DEGs) related mainly to apoptosis and the ER UPR (Fig. 3A). Integration of RNA-seq data and ChIP-seq data showed 33 target genes of XBP1s in NK cells (fig. S4H). Among them, *Pim2* was markedly decreased in NK cells from *Il15*^{Tg}*Xbp1*^{cKO} mice compared with those from *Il15*^{Tg}*Xbp1*$^{f/f}$ mice (Fig. 3B). *Pim2* encodes a proto-oncogene that acts as a serine/threonine protein kinase (41). Prior studies have shown that PIM-2 inhibits apoptosis and promotes cell survival in tumor cells and immune cells (42-44). However, it was not previously recognized as a target of XBP1s. We found significantly lower transcript and protein levels of PIM-2 in NK cells from *Il15*^{Tg}*Xbp1*^{cKO} mice compared with those from *Il15*^{Tg}*Xbp1*$^{f/f}$ mice (Fig. 3, C and D), suggesting that XBP1s may transactivate PIM-2 expression.

When we analyzed the promoter region of *Pim2*, we identified a potential binding site for XBP1s (fig. S4I). Moreover, a strong binding peak of XBP1s at the promoter region of *Pim2* was observed (Fig. 3E). A luciferase reporter assay in both human embryonic kidney (HEK)–293T cells and mouse NK cells showed that XBP1s activated *Pim2* gene transcription (Fig. 3, F and G). Moreover, ChIP-qPCR revealed that the binding of XBP1s to the promoter region of *Pim2* was robustly enriched compared with a normal immunoglobulin G (IgG) control in IL-15–treated *Xbp1*$^{f/f}$ NK cells, but no enrichment was observed in IL-15–treated *Xbp1*^{cKO} NK cells (Fig. 3, H and I, and fig. S4J). This suggests

that XBP1s positively regulates *Pim2* transcription in mouse NK cells by directly binding to the *Pim2* promoter. To confirm that PIM-2 is a functional target of XBP1s in NK cells, we first collected BM cells from *Il15*^{Tg}*Xbp1*$^{f/f}$ and *Il15*^{Tg}*Xbp1*^{cKO} mice and spin-infected them with retrovirus encoding *Pim2*. The infected cells were then transferred into lethally irradiated CD45.1 recipient mice. After 8 weeks, NK cells from recipients were assessed by flow cytometry (Fig. 3J). As predicted, we found that ectopic expression of PIM-2 (fig. S4K) compensated for XBP1 deficiency in NK cells in vivo (Fig. 3K).

An XBP1s–PIM-2 axis controls NK cell survival in humans

To determine whether XBP1s also maintains the survival of human NK cells by targeting PIM-2, we first overexpressed XBP1s in human NK cells. This overexpression of XBP1s significantly increased PIM-2 expression (Fig. 4, A to C). We next found two binding sites for XBP1s in the promoter region of *PIM2* (Fig. 4D). Then, a luciferase reporter assay in HEK-293T cells and human NK cells showed that XBP1s activated *PIM2* gene transcription in the human cells (Fig. 4, E and F). ChIP-qPCR also showed that human XBP1s bound to the *PIM2* promoter (Fig. 4G and fig. S4L). Moreover, overexpression of PIM-2 partly rescued NK cells after treatment with the XBP1s inhibitor 4μ8C in the presence of IL-15, increasing their survival (Fig. 4, H and I). Collectively, our findings reveal a previously unknown XBP1s–PIM-2 axis that regulates NK cell survival in both humans and mice.

PIM-2 stabilizes XBP1s through phosphorylation at Thr^{58}

PIM-2 belongs to a family of serine/threonine protein kinases, and it functions as an oncogene by phosphorylating a wide range of cellular proteins (45, 46). This led us to hypothesize that PIM-2 might phosphorylate and then stabilize XBP1s, the process of which would create a positive feedback loop between PIM-2 and XBP1s in NK cells. We transiently overexpressed FLAG-tagged XBP1s and different doses of hemagglutinin (HA)–tagged PIM-2 in HEK-293T cells. Overexpression of PIM-2 increased protein levels of XBP1s in a dose-dependent manner (Fig. 5A). However, PIM-2 did not enhance endogenous *Xbp1s* mRNA expression (fig. S5A). Given that PIM-2 increases protein levels of XBP1s without increasing its transcription, we examined whether PIM-2 affects the stability of the XBP1s protein. First, we transiently overexpressed FLAG-tagged XBP1s or FLAG-tagged XBP1s plus HA-tagged PIM-2 in HEK-293T cells. Then, we treated the cells with cycloheximide (CHX) to inhibit global protein translation. The presence of PIM-2 significantly delayed the degradation of XBP1s (Fig. 5, B and C), indicating that PIM-2 increases the amount of XBP1s protein by enhancing stability. Because XBP1s degradation is mediated by ubiquitination and proteasomes (12), we then examined the effect of coexpressing PIM-2 and XBP1s. Ubiquitination of XBP1s was reduced by the coexpression compared with that in control cells that expressed vector instead of PIM-2 (Fig. 5D). This finding indicates that PIM-2 inhibits the ubiquitination of XBP1s, thereby suppressing proteasomal degradation.

This reduced ubiquitination prompted us to hypothesize that PIM-2 stabilizes XBP1s by phosphorylation. To test this idea, we transfected FLAG-tagged XBP1s and HA-tagged PIM-2 into HEK-293T cells. Reciprocal coimmunoprecipitation (co-IP) data revealed an interaction between XBP1s and PIM-2, because PIM-2 was coprecipitated with XBP1s (Fig.

5E) and vice versa (Fig. 5F). In addition, XBP1s also precipitated endogenous PIM-2 in IL-15–treated mouse and human NK cells (Fig. 5, G and H), indicating that PIM-2 stabilizes XBP1s by direct modification. We then determined whether PIM-2 could phosphorylate XBP1s. Compared with the empty vector control, transfection of PIM-2 increased serine/threonine phosphorylation levels of XBP1s, as detected by immunoblotting with phospho-Thr/Ser–specific antibodies (Fig. 5I). Thus, PIM-2 enhanced Ser/Thr phosphorylation of XBP1s and increased its stability.

To determine which residues on XBP1s are phosphorylated by PIM-2, we cotransfected FLAG-tagged XBP1s and HA-tagged PIM-2 [wild type (WT) or kinase-dead (KD) PIM-2, K61A] into HEK-293T cells (45). Compared with the PIM-2–KD or vector control, transfection of WT PIM-2 increased XBP1s phosphorylation on threonine residues, as detected by immunoblotting with a phospho-Thr–specific antibody (Fig. 5J). However, PIM-2 did not affect phosphorylation levels of serine residues in XBP1s (Fig. 5K). Because prior studies had identified a consensus substrate motif for PIM-2, R-X-R-H-X-pS/T (47), we performed in silico analyses for potential PIM-2 substrate motifs in XBP1s. We identified one putative PIM-2 phosphorylation site (Thr^{58}) in XBP1s (fig. S5B) and then found that mutating Thr^{58} (T58A) significantly reduced PIM-2–induced XBP1s phosphorylation (Fig. 5L). To determine whether PIM-2 stabilizes XBP1s by phosphorylating it at Thr^{58}, we cotransfected XBP1s-WT or XBP1s-T58A with HA-tagged PIM-2 and then treated with CHX. PIM-2 was not able to stabilize this mutant XBP1s as effectively as it stabilized WT XBP1s (Fig. 5M). This suggests that Thr^{58} is a critical phosphorylation site that contributes to the stabilization of XBP1s by PIM-2 kinase. Together, our data suggest that PIM-2 stabilizes XBP1s by phosphorylating it at Thr^{58}.

PIM-2 is essential for NK cell development and homeostasis in mice

PIM-2 plays a critical role in regulating cell survival and proliferation in cancer cells (44, 48, 49). Prior studies reported that PIM-2 negatively regulates $Foxp3^{+}$ regulatory T cells and T cell responses in transplantation and tumor immunity (42, 50). We evaluated the role of PIM-2 in NK cell development and homeostasis using PIM-2 KO mice (42, 51). We found that the percentages and absolute numbers of NK cells were significantly decreased in the spleens and BM from PIM-2 KO mice compared with those from WT mice (fig. S5, C and D), which is consistent with a prior report (42), indicating that PIM-2 positively affects NK cell homeostasis at steady state. To further explore whether PIM-2 affects NK cell development, we examined the hematopoietic stem cells (HSCs) and NK cell progenitors in the BM. PIM-2 deficiency significantly reduced the percentages and absolute numbers of HSCs, pre-NK cell progenitors (preNKPs), and refined NKPs (rNKPs) but markedly increased percentages and absolute numbers of common lymphoid progenitors (CLPs) in the BM (fig. S5E), indicating that PIM-2 regulates NK cell development likely at the transition from CLP to preNKP stage. However, further studies are warranted to reveal the detailed mechanism by which PIM-2 regulates NK cell development and homeostasis.

XBP1 deficiency impairs NK cell effector functions and antitumor immunity

We have shown that $Xbp1^{cKO}$ mice displayed more tumor metastasis compared with $Xbp1^{f/f}$ mice in association with decreased tumor-infiltrating NK cells (Fig. 1C and fig.

S1C). However, whether XBP1 regulates NK cell effector functions remains undetermined in mice. We found that XBP1 deficiency impairs IFN-γ production by NK cells in the settings of cytokine costimulation with IL-12 plus IL-18 or in the presence of a tumor cell line (YAC-1) (fig. S6, A and B). In contrast, NK cells from *Xbp1*$^{f/f}$ and *Xbp1*^{cKO} mice have similar low baseline levels of IFN-γ production in the absence of this stimulation (fig. S6C). We then assessed the functional capacity of XBP1-deficient NK cells on the *Il15*^{Tg} background. NK cells from *Il15*^{Tg}*Xbp1*^{cKO} mice produced less granzyme B and perforin compared with those from *Il15*^{Tg}*Xbp1*$^{f/f}$ mice (Fig. 6, A and B), and IFN-γ production was significantly decreased (Fig. 6C). After activation with IL-15, moreover, NK cells from *Il15*^{Tg}*Xbp1*^{cKO} mice had less cytotoxicity against YAC-1 cells than those from *Il15*^{Tg}*Xbp1*$^{f/f}$ mice (Fig. 6D). Also, we found a larger number of B16-F10 melanoma tumor metastases in *Il15*^{Tg}*Xbp1*^{cKO} mice than in *Il15*^{Tg}*Xbp1*$^{f/f}$ mice (Fig. 6E). Last, an NK depletion assay showed that the antitumor effect of XBP1s was NK cell–dependent (Fig. 6F). Collectively, our findings indicate that XBP1 also controls NK cell effector functions upon certain types of activation.

XBP1s promotes IFN-γ production by recruiting T-bet to the promoter region of *Ifng*

We previously showed that XBP1s positively regulates human NK cell effector functions by enhancing the expression of IFN-γ and granzyme B (26). However, the mechanism has not been fully unraveled. We therefore analyzed the expression of genes encoding molecules related to NK cell effector functions, including *Ifng* (IFN-γ), *Gzmb* (granzyme B), and *Prf1* (perforin), in NK cells from *Il15*^{Tg}*Xbp1*$^{f/f}$ or *Il15*^{Tg}*Xbp1*^{cKO} tumor-bearing mice. mRNA levels of *Ifng* and *Gzmb*, but not *Prf1*, were significantly lower in NK cells from *Il15*^{Tg}*Xbp1*^{cKO} tumor-bearing mice than in those from*Il15*$^{Tg-}$ *Xbp1*$^{f/f}$ tumor-bearing mice (Fig. 7, A to C). These murine data are consistent with our findings with human NK cells, indicating that XBP1s controls NK cell effector functions, most likely by positively regulating IFN-γ and granzyme B.

Our previous study showed that XBP1s binds directly to the *GZMB* promoter to enhance the transcription of *GZMB* via T-BET in human NK cells (26). To determine whether XBP1s behaves similarly in mice, we performed a luciferase reporter assay, finding that mouse XBP1s activated *Gzmb* gene transcription (Fig. 7D), as in human NK cells. We also found a strong binding peak of XBP1 in the promoter region of *Gzmb* in mouse NK cells (fig. S7A). Within 2 kb of the promoter upstream of the mouse or human *Ifng/IFNG* gene transcription start site, 11 and 4 XBP1 binding sites were identified, respectively. However, very weak binding peaks were found around the promoter region of *Ifng* in mouse NK cells (fig. S7B). Using a luciferase reporter assay, we found that XBP1s did not activate *Ifng/IFNG* transcription in either mouse or human cells (fig. S7, C and D), suggesting that XBP1s does not directly regulate *Ifng/IFNG* expression.

We therefore turned our attention to the transcription factor T-bet (encoded by *Tbx21*), the master regulator of IFN-γ expression in T cells and NK cells (52, 53). We previously showed that XBP1s can interact with T-BET in human NK cells and that it regulates the transcription of *GZMB* by binding to that gene′s promoter (26). To investigate whether mouse XBP1s could directly promote the transcription of *Tbx21*, we used luciferase reporter

assays and found that XBP1s does not promote transcription by interacting with the *Tbx21/TBX21* promoter in either mouse or human cells (fig. S7, E and F). ChIP-seq data also demonstrated that XBP1 has no binding peaks around the promoter region of *Tbx21* in mouse NK cells (fig. S7G). Moreover, XBP1s also did not bind to the *Tbx21* enhancer element (fig. S7H), a conserved sequence 12 kb upstream of the transcription start site that regulates *Tbx21* expression (54). Therefore, XBP1s does not appear to promote IFN-γ expression by increasing T-bet/T-BET expression.

We therefore proposed that XBP1s might promote IFN-γ expression via the same mechanism that it uses to recruit T-bet to the promoter of *Ifng* as it regulates the expression of human GZMB (26). After we cotransfected mouse XBP1s and T-bet into HEK-293T cells, we found significantly higher transcriptional activity of *Ifng* than in cells transfected with XBP1s alone or T-bet alone (Fig. 7E). A similar difference was observed between human XBP1s and T-BET (Fig. 7F). Moreover, we performed luciferase reporter assays in mouse and human NK cells and observed similar results (Fig. 7, G and H). Co-IP followed by immunoblotting using antibody to XBP1s showed that XBP1s interacts with T-bet/T-BET in IL-15–activated mouse/human NK cells (Fig. 7, I and J). To further prove our hypothesis that XBP1 promotes IFN-γ production by recruiting T-bet/T-BET to the promoter region of *Ifng/IFNG*, we used antibodies against XBP1s or T-bet/T-BET to separately precipitate the cross-linked DNA-protein complexes in IL-15–activated mouse and human NK cells and analyzed the binding of the XBP1s/T-bet complex to the *Ifng/IFNG* promoter by ChIP-qPCR. Our results revealed that the DNA immunoprecipitated by anti-XBP1s or anti–T-bet/T-BET contained the *Ifng/IFNG* promoter. The *Ifng/IFNG* promoter DNA amount immunoprecipitated by anti-XBP1s or anti–T-bet/T-BET was significantly higher than that immunoprecipitated by an IgG control antibody in both mouse/human NK cells (Fig. 7, K and L). The binding of T-bet and T-BET to the *Ifng* or *IFNG* promoter, respectively, served as control (Fig. 7, K and L). Last, to confirm that T-bet is a functional target of XBP1s in mouse NK cells, we spin-infected NK cells from *Xbp1*^{cKO} mice with lentivirus encoding T-bet (Fig. 7M). As predicted, we found that ectopic expression of T-bet partly compensated for the defect in IFN-γ production when XBP1s-deficient NK cells were treated with IL-12 plus IL-15 (Fig. 7N). Together, our data suggest that XBP1s promotes IFN-γ production by recruiting T-bet to the promoter region of *Ifng*.

DISCUSSION

IL-15 is a dominant regulator of NK cell survival and effector functions (4, 33, 55, 56). However, the molecular mechanisms that underlie this remain poorly understood. In this study, we provide genetic evidence that IL-15–XBP1s signaling controls NK cell survival and effector functions through two targets: PIM-2 and T-bet. XBP1s binds to the promoter of *Pim2* and induces its expression to maintain NK cell survival. In turn, PIM-2 stabilizes XBP1s protein through phosphorylation, creating a positive feedback loop. This permits the downstream interaction between XBP1s and T-bet, thereby promoting granzyme B and IFN-γ production (fig. S8). Thus, our present study, together with our prior report (26), confirms that XBP1s plays an indispensable role in IL-15–mediated cell survival and effector functions in NK cells.

XBP1s has a short half-life because it is rapidly degraded by proteasomes. In human NK cells, IL-15 stabilizes XBP1s by phosphorylating AKT, which is upstream of XBP1s. Phosphorylated AKT then inhibits the ubiquitination of XBP1s, maintaining its stability (26). Here, we found that the stability of XBP1s can also be regulated by its downstream target, PIM-2, which creates a positive feedback loop. In particular, PIM-2 interacts with XBP1s physically and phosphorylates the latter at the Thr^{58} residue. Collectively, our findings reveal that NK cells have at least two mechanisms for stabilizing XBP1s after the cells are activated by IL-15. These mechanisms are responsible for the survival and functioning of IL-15–activated NK cells.

In resting cells, in the absence of ER stress, XBP1 is maintained in an inactive state. It has been reported that XBP1 is not required for homeostasis, development, or effector function of T cells or dendritic cells (DCs) at steady state (21, 57) but is essential to control the function of T cells or tumor-associated DCs under conditions of tumor challenge (21, 22). We and others have shown that XBP1s is inactivated in resting NK cells but can be activated by IL-15 and MCMV infection (26, 27). In the current study, although we confirm that XBP1 does not affect NK cell homeostasis and maturation at steady state, our findings reveal that the endogenous XBP1 is important for NK cell survival and effector functions under conditions of excessive IL-15, tumor challenge, and inflammation.

It was previously reported that XBP1s drives NK cells to proliferate and expand after MCMV infection by transactivating c-MYC (27). However, our current study demonstrates that XBP1s uses PIM-2 signaling to control NK cell survival but not proliferation in response to IL-15. This indicates that activation of IRE1α-XBP1 signaling not only is regulated by different upstream regulators but also has different targets depending on the initial stimulus. Therefore, it is necessary to identify and distinguish the exact target genes of XBP1s in NK cells under specific conditions. Furthermore, overexpression of PIM-2 cannot completely rescue the loss of NK cells due to deficiency of XBP1; we acknowledge that other mechanisms beyond PIM-2 may be involved in XBP1s-mediated survival of NK cells. Last, our study indicates that PIM-2 is essential for NK cell homeostasis in mice likely by regulating NK cell development at the transition from the CLP stage to the preNKP stage. Further studies are warranted to reveal the associated mechanism.

Recently, NK cell–based therapies, such as CAR-NK, have attracted attention because of their allogeneic, off-the-shelf potential for treating cancer (5, 58). Although there are no direct binding sites for XBP1s on the *Ifng* promoter, we found that XBP1s interacts with T-bet to enhance T-bet's binding to that promoter, thereby promoting NK cell activity. We therefore believe that future studies are warranted to evaluate whether manipulating NK cells to overexpress XBP1 could be a practical and effective approach for treating certain forms of cancer.

In conclusion, we show here that XBP1s is a crucial transcription factor that acts downstream of IL-15 signaling to control two of NK cells' most important features—survival and effector functions—in animal models and human cells. Thus, targeting the IL-15–XBP1s–PIM-2 signaling pathway may be a promising strategy for advancing NK cell–based therapies against tumors.

MATERIALS AND METHODS

Study design

The aim of this study was to explore the role and detailed mechanisms by which IL-15–XBP1s signaling controls survival and effector functions of NK cells. This was achieved using *Xbp1*^{cKO} mice and *Il15*^{Tg}*Xbp1*^{cKO} compound mice; a tumor melanoma model; an EAE model; BM chimeras; and several biochemistry experiments, such as RNA-seq, ChIP assay and co-IP assay, flow cytometric analysis, quantitative real-time reverse transcription PCR (RT-PCR) analysis, ex vivo cytotoxicity assay, etc. Outcomes were presented as NK cell percentages, numbers, survival, and effector functions, etc. All data points generated were included in the analysis. For in vitro studies, as least three independent experiments were performed. For in vivo studies, mice were randomly assigned for experiments. The sample size is specified in each figure legend. The experiments were performed unblinded.

Mice

Xbp1$^{fl/fl}$ mice were generated in the laboratory of L. H. Glimcher (Harvard Medical School) as previously described (30). *Ncr1*-iCre mice were provided by E. Vivier (Centre d′Immunologie de Marseille-Luminy) (31). IL-15 Tg (*Il15*^{Tg}) mice were generated by our group and backcrossed into the C57BL/6 background (32, 33). *Il15*^{Tg}*Xbp1*^{cKO} mice were generated by crossing *Il15*^{Tg} mice with *Xbp1*^{cKO} mice in the animal facility at City of Hope. NCI B6-Ly5.1/Cr (CD45.1) mice were purchased from Charles River Laboratories. PIM-2 KO mice were provided by X. Yu (Medical College of Wisconsin) and A. Berns (Netherlands Cancer Institute) (42). All experimental mice were bred and maintained under specific pathogen–free conditions. Six- to 12-week-old male or female mice were used for the experiments. Age- and sex-matched Cre-negative littermates were used as controls. All animal experiments were approved by the City of Hope Institutional Animal Care and Use Committee.

Human peripheral blood samples

Peripheral blood samples from de-identified healthy donors were obtained from the Michael Amini Transfusion Medicine Center of City of Hope National Medical Center under institutional review board–approved protocols.

Lung metastatic melanoma model

Cells from the murine melanoma cell line B16F10 were cultured in Dulbecco’s modified Eagle′s medium (Gibco) supplemented with 10% fetal bovine serum (FBS; Gibco). B16F10 cells (2×10^5) were injected intravenously into mice. Fourteen days after injection, the mice were euthanized for postmortem analysis. Metastatic nodules in the lung were analyzed macroscopically and counted. For NK cell depletion, mice were injected intraperitoneally with 200 μg of anti-NK1.1 antibody (clone PK136, Bio X Cell) on days 0 and 7 after tumor inoculation.

EAE model

EAE was induced in 12-week-old female *Xbp1*$^{f/f}$ and *Xbp1*^{cKO} mice using the Hooke Kit $MOG_{35–55}$/CFA Emulsion PTX kit (catalog no. EK-2110, Hooke Laboratories) according to the manufacturer's protocol. In brief, mice were immunized with an emulsion of myelin oligodendrocyte glycoprotein peptide ($MOG_{35–55}$) in complete Freund's adjuvant (CFA) by subcutaneous injection into two different sites (100 μl of emulsion per site) on each hind flank, followed by intraperitoneal administration of 100 μl of pertussis toxin (PTX) in phosphate-buffered saline (PBS) after 2 hours of $MOG_{35–55}$ immunization. PTX (100 μl) was given again 24 hours later. The mice were monitored for clinical symptoms of EAE daily from 9 to 18 days after immunization. EAE was scored on a scale of 0 to 5 based on the grading system for clinical assessment of EAE as described previously (59).

Flow cytometry

Single-cell suspensions were prepared from the BM, spleens, lungs, and tumor tissues of mice as described previously (33). The following fluorescence dye–labeled antibodies were used in this study: BV510-CD3ε (145-2C11, BioLegend), phycoerythrin (PE)–CD3ε (145-2C11, BioLegend), PE/Cy7-CD3ε (145-2C11, BioLegend), BV510-NK1.1 (PK136, BioLegend), allophycocyanin (APC)–Cy7-NK1.1(PK136, BioLegend), APC/Fire 750-NK1.1 (PK136, BioLegend), fluorescein isothiocyanate (FITC)–NKp46 (29A1.4, BioLegend), BV421-CD11b (M1/70, BioLegend), APC/Cy7-CD27 (LG.3A10, BioLegend), PE–IFN-γ (XMG1.2, BioLegend), PE/Cy7–granzyme B (QA16A02, BioLegend), APC-perforin (S16009A, BioLegend), PE–annexin V (BioLegend), Alexa Fluor 488–Ki67 (11F6, BioLegend), BUV395-Ki67 (B56, BD Biosciences), PE-FasL (MFL3, BioLegend), PE-TRAIL (N2B2, BioLegend), FITC–c-kit (2B8, BioLegend), BV510–Sca-1 (D7, BioLegend), PE-FLT3 (A2F10.1, BD Biosciences), and BV-786-CD122 (5H4, BD Biosciences). To evaluate mouse NK cell proliferation, we labeled cells with 5 μM CellTrace Violet (Invitrogen) according to the manufacturer's protocol. Intracellular staining of Ki67 was performed by fixing and permeabilizing with the Foxp3/Transcription Factor Staining Kit (eBioscience). In vitro BrdU labeling was performed using the FITC BrdU Flow Kit (BD Biosciences) according to the manufacturer's protocol. In vivo EdU labeling was performed using the Click-iT EdU Alexa Fluor 488 Flow Cytometry Assay Kit (Invitrogen) according to the manufacturer's protocol. In brief, mice were intraperitoneally injected with 2 mg of EdU in PBS, and EdU labeling was examined 16 hours later using the Click-iT EdU Assay kit. For IFN-γ staining, cells were stimulated with IL-12 (10 ng/ml) plus IL-18 (10 ng/ml) or YAC-1 cells at the effector-to-target ratio of 10:1 for 16 hours (BioLegend). Cells were stained with the indicated cell surface markers and fixed/permeabilized using the Fixation/Permeabilization Kit (BD Biosciences). Flow cytometry analysis was performed on BD LSRFortessa X-20 (BD Biosciences). Data were analyzed using NovoExpress Software (Agilent Technologies). The antibodies used are listed in table S1.

NK cell isolation, culture, transduction, and treatment

Mouse NK cells were isolated from the spleens of mice using the EasySep Mouse NK Cell Isolation Kit (STEMCELL Technologies) as previously described (33). Human NK cells were enriched using RosetteSep Human NK Cell Enrichment Cocktail (STEMCELL

Technologies) and Ficoll-Paque (GE Healthcare). Both mouse and human NK cells were cultured in RPMI 1640 with 10% heat-inactivated FBS (Gibco) at 37°C in a 5% CO_2 humidified incubator in the presence of IL-2 (100 U/ml; catalog no. Bulk Ro 23-6019, National Cancer Institute). For human NK cell transduction, human XBP1s cDNA or *PIM2* cDNA was cloned into the pCDH-CMV-MCS-EF1-copGFP lentivirus vector (System Biosciences). Empty, XBP1s-expressing, or PIM-2–expressing lentiviruses were produced in HEK-293T cells with psPAX2 packaging (Addgene) and pMD2.G envelope plasmid DNA (Addgene) using PEI MAX (Polysciences) according to the manufacturer's instructions. Concentrated lentivirus was added to NK cells cultured in RPMI medium 1640 supplemented with 10% FBS and polybrene (10 μg/ml) with 2000*g* centrifugation for 2 hours. Cells were cultured for an additional 48 hours. Green fluorescent protein (GFP)–positive cells were sorted using BD FACSAria Fusion (BD Biosciences). Sorted GFP-positive NK cells were pretreated with 4μ8C (50 μM/ml) for 1 hour, washed twice with RPMI 1640, and then cultured with IL-15 (50 ng/ml). Live cells were counted on days 3, 5, and 7 after IL-15 treatment. For mouse NK cell transduction, mouse *Tbx21* cDNA was cloned into the pCDH-CMV-MCS-EF1-copGFP lentivirus vector (System Biosciences). Empty or T-bet–expressing lentiviruses were produced as described above. Mouse NK cells were transduced with concentrated lentivirus through centrifugation. GFP-positive NK cells were sorted 48 hours after transduction and treated with IL-12 (10 ng/ml) plus IL-15 (10 ng/ml) for 24 hours. The cells were then collected for flow cytometry analysis.

In vivo mouse treatment with IL-15

Mice were intraperitoneally injected with 2 μg of recombinant human IL-15 (catalog no. 745101, National Cancer Institute) for 5 days. They were then euthanized for flow cytometric analysis.

Quantitative real-time RT-PCR

RNA was isolated using the RNeasy Mini Kit (QIAGEN) and then reverse-transcribed to cDNA with the PrimeScript RT Reagent Kit with gDNA Eraser (Takara Bio) following the manufacturer's instructions. mRNA expression levels were analyzed using SYBR Green PCR Master Mix and the QuantStudio 12K Flex Real-Time PCR System (both from Thermo Fisher Scientific). Primer sequences are listed in table S2.

Immunoblotting

Immunoblotting was performed according to standard procedures as previously described (33). The following antibodies were used: Xbp1s (ab220783, Abcam), Xbp1s [catalog no. 40435, Cell Signaling Technology (CST)], XBP1s (647502, BioLegend), Pim-2 (4730, CST), Pim-2 (ab129057, Abcam), T-bet (13232, CST), anti-FLAG M2-peroxidase [horseradish peroxidase (HRP)] (A8592, Sigma-Aldrich), anti-HA–peroxidase antibody (H6533, Sigma-Aldrich), ubiquitin (58395, CST), phosphoserine/threonine-phenylalanine antibody (9631, CST), phosphothreonine (42H4) (9386, CST), phosphoserine antibody (PSR-45) (NB600-405, Novus Biologicals), β-actin (catalog no. 66009-1-Ig, Proteintech), and β-tubulin (2128, CST). The protein bands were detected using a SuperSignal West Pico Plus chemiluminescence ECL kit (Thermo Fisher Scientific) and imaged with FluorChem E system (Protein Simple) or detected with IRDye secondary antibody (Li-COR Biosciences)

and visualized with Odyssey CLx Imager (Li-COR Biosciences). Densitometric analysis was performed to quantify intensity of immunoblot bands using ImageJ. The antibodies used are listed in table S1.

RNA sequencing

Total RNA was isolated from sorted purified splenic NK cells from *Il15*^{Tg}*Xbp1*$^{f/f}$ and *Il15*^{Tg}*Xbp1*^{cKO} mice using the RNeasy Mini Kit (QIAGEN). RNA libraries were generated using the KAPA Hyper Prep Kit (KAPA Biosystems). Sequencing was performed at the City of Hope Genomics Facility on an Illumina HiSeq2500 machine with single-read 50–base pair (bp) mode. Sequencing reads were mapped to the mouse genome using HISAT2 (version v101). Transcript counts were generated using HTSeq, and differential gene analysis was performed using DESeq2. DEGs from RNA-seq are listed in table S3.

Plasmids

An *Xbp1s* cDNA open reading frame clone with FLAG-tag at the C terminus was purchased from GenScript (clone ID: OMu19236). Amplified XBP1s cDNA was cloned into the pCDH-CMV-MCS-EF1α-copGFP lentivirus vector (System Biosciences) to generate pCDH-XBP1s-FLAG. XBP1s (T58A) with a C-terminal FLAG-tag was synthesized by Twist Bioscience and cloned into a pCDH vector. Mouse *Pim2* was PCR-amplified from mouse NK cells to add an HA-tag at the N terminus. Then, it was inserted into the pCDH vector. Human *PIM2* and mouse *Tbx21* were cloned into the pCDH vector. KD PIM-2 (K61A) with an N-terminal HA-tag was synthesized by Twist Bioscience and cloned into the pCDH vector. The pCMV-8xHis-Ub plasmid was purchased from Addgene (#107392).

Luciferase reporter assay

Mouse *Pim2, Gzmb*, and *Ifng* and human *PIM2* and *IFNG* promoter regions ranging from −2000 to +100 bp of the transcription start site were cloned into a pGL4-basic luciferase reporter vector (Promega) to generate the pGL4 reporter plasmid. The human and mouse *TBX21/Tbx21* reporter plasmids and the *Tbx21* enhancer reporter plasmid were generated as previously described (60). HEK-293T cells purchased from the American Type Culture Collection (ATCC) were cotransfected with the reporter plasmids and with XBP1s or T-bet overexpression plasmids or empty vector together with a pRL-TK renilla reporter plasmid (Promega) to normalize transfection efficiency. The cells were harvested for lysis 24 hours after transfection, and luciferase activity was quantified fluorimetrically with the Dual-Luciferase System (Promega). Luciferase reporter assay in primary NK cells was performed as previously described (61, 62). IL-2–expanded mouse NK cells were starved for 12 hours before transfection. The promoter and/or expression plasmids (2 μg each) and pRL-TK (500 ng) were electroporated into 5×10^6 starved mouse NK cells or primary human NK cells with the Amaxa Human NK Cell Nucleofector Kit (Lonza) and an Amaxa nucleofector device (Amaxa) with program U-001 according to the manufacturer's instructions. Cells were harvested at 4 hours after transfection, and lysates were analyzed for luciferase activity using the Dual-Luciferase System (Promega).

ChIP-seq and ChIP-qPCR

ChIP assays were carried out using a Pierce Magnetic ChIP Kit (catalog no.26157, Thermo Fisher Scientific) according to the manufacturer's instructions. Briefly, 5×10^6 purified mouse primary NK cells or human NK cells were pretreated with IL-15 (50 ng/ml) for 1 hour. The cells were then cross-linked with fresh 1% formaldehyde (Thermo Fisher Scientific) for 10 min at room temperature (RT) and quenched with 125 mM glycine for 5 min at RT. Cells were washed three times in cold PBS containing protease inhibitors. Nuclei were isolated using the SimpleChIP Enzymatic Chromatin IP Kit (#91820, CST), and chromatin was sheared on ice using a Fisher sonic dismembrator with the setting of 10 cycles of 4 s "on" and 8 s "off." The input fraction (2%) was saved, and the remaining sheared chromatin was used for ChIP with a rabbit anti-Xbp1s antibody (catalog no. 40435, CST) or rabbit anti–T-bet antibody (97135, CST) or an IgG isotype control (Millipore) in 1× ChIP buffer with rotation overnight at 4°C. Protein G magnetic beads were added to each immunoprecipitation and incubated for 2 hours at 4°C with rotation. The chromatin bead antibody complexes were then washed three times with low-salt wash buffer and one-time with high-salt wash buffer. Chromatin was then eluted using 1% SDS in Tris-EDTA. Cross-linking was reversed by incubation with 5 M NaCl and proteinase K at 65°C overnight. DNA was purified with a ChIP DNA Clean & Concentrator kit (Zymo Research). ChIP-seq libraries were prepared using a KAPA Hyper DNA kit (Roche) and sequenced on an Illumina NovaSeq 6000 platform with 100-bp paired-end reads at the Translational Genomics Research Institute (TGen).

Paired-end reads were obtained for the two replicates. All reads were trimmed with Trim Galore v0.6.7 and subjected to quality control with FastQC v0.11.9 before and after adaptor trimming (63). After trimming, the reads were then mapped to the mouse genome (GRCm38/mm10) using Bowtie2 v2.4.5 (64). Peak calling for each ChIP replicate to the input DNA was performed using MACS2 v2.2.7.1 (65). The peaks were annotated to mm10 genomic features using the annotatePeaks.pl function from HOMER v4.11.1, and the motifs enriched in ChIP peaks were analyzed with the findMotifsGenome.pl function from HOMER v4.11 (http://homer.ucsd.edu/homer/motif/). ChIP peaks were visualized using Integrative Genomics Viewer software (www.igv.org). KEGG pathway enrichment analysis of peaks was performed using DAVID (https://david.ncifcrf.gov/). The DNA immunoprecipitated by the indicated antibodies was analyzed with qPCR. The sequences of all primers are listed in table S1.

Coimmunoprecipitation

Cells were lysed in lysis buffer [10% glycerol, 50 mM Hepes-KOH (pH 7.5), 100 mM KCl, 2 mM EDTA, 0.1% NP-40, 10 mM NaF, 0.25 mM Na_3VO_4, 50 mM β-glycerophosphate, 2 mM dithiothreitol, and 1× protease and phosphatase inhibitor cocktail] and were incubated on ice for 15 min. Cell lysates were centrifuged at 14,000*g* for 20 min at 4°C, and supernatants were collected. Cell lysates (about 5 mg per sample) were incubated with antibody (5 μg per sample) or 20 μl of Pierce Anti-HA Magnetic Beads (88836, Thermo Fisher Scientific) or Anti-FLAG M2 Magnetic Beads (M8832, Sigma-Aldrich) overnight at 4°C with gentle rotation. Dynabeads Protein A (20 μl) (10001D, Invitrogen) was added to the tubes, which were rotated at RT for 1 hour. Beads were separated out with a magnet and

washed three times with cold lysis buffer. Fifty microliters of 50 mM glycine (pH 2.8) were added to the beads, which were incubated at RT on a rotator for 10 min to elute the protein. The beads were magnetically separated, and the supernatants containing the target antigen were saved. Ten microliters of neutralization buffer [0.5 M Tris (pH 7.5) and 1.5 M NaCl (pH 8.0) solution] were added for each 50 μl of eluate. The eluate was resuspended in 4× LDS Sample Buffer (Invitrogen) and incubated at 70°C for 10 min. The supernatants were then collected and used for immunoblotting.

Protein degradation assay

HEK-293T cells were transfected with XBP1s-FLAG alone or with PIM-2–HA. After 24 hours of transfection, the cells were treated with the translation inhibitor CHX (20 μg/ml, Sigma-Aldrich). Cells were collected at 0.25, 0.5, 1, 2, and 4 hours after CHX incubation. Cells without treatment were dubbed 0 hours. Protein levels of XBP1s were determined by immunoblotting and subsequently quantified with ImageJ software.

Ex vivo cytotoxicity assay

Ex vivo cytotoxicity of NK cells was evaluated by standard ^{51}Cr release assays. The mouse T cell lymphoma cell line YAC-1 (ATCC) was used for target cells. Mice were intraperitoneally injected with polyinosinic:polycytidylic acid [poly(I:C); 200 μg/mice] for 18 hours. Poly(I:C)-activated NK cells were isolated from the spleen using the EasySep Mouse NK Cell Isolation Kit (STEMCELL Technologies). Purified NK cells were cocultured with target cells at a ratio of 5:1, 2.5:1, and 1.25:1 in the presence of IL-2 (50 U/ml).

Retroviral transduction and BM chimeras

Mouse *Pim2* cDNA was cloned into the MSCV-IRES-GFP plasmid. Empty or PIM-2–expressing retroviruses were produced in GP2-293 cells with pCL-Eco packaging plasmid (Addgene), using PEI MAX (Polysciences) according to the manufacturer's instructions. BM for transduction was isolated by flushing femurs and tibias from *Il15*^{Tg}*Xbp1*$^{f/f}$ and *Il15*^{Tg}*Xbp1*^{cKO} mice 4 days after treatment with 5 mg of 5-fluorouracil (Sigma-Aldrich). BM cells (2×10^6/ml) were seeded in a 24-well plate in 1 ml of culture medium and 1 ml of retroviral supernatants supplemented with polybrene (10 μg/ml; EMD Millipore). Cells were spin-infected at 230*g* for 1.5 hours at 32°C and then incubated at 37°C for 4 to 6 hours. Transduced BM cells were washed twice and cultured in Iscove's modified Dulbecco's medium + 15% FBS + 1× penicillin/streptomycin + stem cell factor (50 ng/ml) + IL-3 (20 ng/ml) + IL-6 (10 ng/ml) (PeproTech). Three days later, cells were washed and transferred to a lethally irradiated CD45.1 congenic recipient. Eight weeks later, NK cells were isolated from the spleen for flow cytometry analysis.

Statistical analysis

Data are presented by descriptive statistics such as means ± SD. For continuous end points such as flow cytometry data or RT-PCR data, a Student's *t* test or paired *t* test was used to compare two independent or matched conditions/groups, and one-way analysis of variance (ANOVA) models were used to compare three or more independent conditions/groups. Two-

way ANOVA models were used to assess the interaction effects between two factors (2 × 2), followed by post hoc group comparisons. Linear mixed models (i.e., two-way ANOVA with mixed-effects models in PRISM) were used to account for the variance-covariance structure due to repeated measures such as tumor volume. All tests were two-sided. P values were adjusted for multiple comparisons by the Holm-Šídák procedure. $P < 0.05$ was considered statistically significant. *$P < 0.05$, **$P < 0.01$, ***$P < 0.001$, and ****$P < 0.0001$. Prism software v.9.0 (GraphPad) and SAS v.9.4 (SAS Institute) were used to perform statistical analyses.

Supplementary Material

Refer to Web version on PubMed Central for supplementary material.

Acknowledgments:

We thank L. H. Glimcher (Harvard Medical School) for providing *Xbp1*$^{fl/fl}$ mice and E. Vivier (Centre d'Immunologie de Marseille-Luminy) for providing *Ncr1*-iCre mice. We thank X. Yu (Medical College of Wisconsin) and A. Berns (Netherlands Cancer Institute) for providing PIM-2 KO mice.

Funding:

This work was supported by grants from the NIH (CA247550, NS106170, AI129582, CA265095, CA210087, CA264512, CA266457, and CA163205), the Leukemia & Lymphoma Society (1364-19), and a 2021 Exceptional Project Award from the Breast Cancer Alliance.

REFERENCES AND NOTES

1. Spits H, Bernink JH, Lanier L, NK cells and type 1 innate lymphoid cells: Partners in host defense. Nat. Immunol 17, 758–764 (2016). [PubMed: 27328005]
2. Sun JC, Lanier LL, NK cell development, homeostasis and function: Parallels with CD8$^+$ T cells. Nat. Rev. Immunol 11, 645–657 (2011). [PubMed: 21869816]
3. Myers JA, Miller JS, Exploring the NK cell platform for cancer immunotherapy. Nat. Rev. Clin. Oncol 18, 85–100 (2021). [PubMed: 32934330]
4. Ma S, Caligiuri MA, Yu J, Harnessing IL-15 signaling to potentiate NK cell-mediated cancer immunotherapy. Trends Immunol. 43, 833–847 (2022). [PubMed: 36058806]
5. Yilmaz A, Cui H, Caligiuri MA, Yu J, Chimeric antigen receptor-engineered natural killer cells for cancer immunotherapy. J. Hematol. Oncol 13, 168(2020). [PubMed: 33287875]
6. Ma R, Lu T, Li Z, Teng KY, Mansour AG, Yu M, Tian L, Xu B, Ma S, Zhang J, Barr T, Peng Y, Caligiuri MA, Yu J, an oncolytic virus expressing il15/il15rα combined with off-the-shelf EGFR-CAR NK cells targets glioblastoma. Cancer Res. 81, 3635–3648 (2021). [PubMed: 34006525]
7. Hetz C, The unfolded protein response: Controlling cell fate decisions under ER stress and beyond. Nat. Rev. Mol. Cell Biol 13, 89–102 (2012). [PubMed: 22251901]
8. Harding HP, Zhang Y, Ron D, Protein translation and folding are coupled by an endoplasmic-reticulum-resident kinase. Nature 397, 271–274 (1999). [PubMed: 9930704]
9. Cox JS, Shamu CE, Walter P, Transcriptional induction of genes encoding endoplasmic reticulum resident proteins requires a transmembrane protein kinase. Cell 73, 1197–1206 (1993). [PubMed: 8513503]
10. Haze K, Yoshida H, Yanagi H, Yura T, Mori K, Mammalian transcription factor ATF6 is synthesized as a transmembrane protein and activated by proteolysis in response to endoplasmic reticulum stress. Mol. Biol. Cell 10, 3787–3799 (1999). [PubMed: 10564271]
11. Bertolotti A, Zhang Y, Hendershot LM, Harding HP, Ron D, Dynamic interaction of BiP and ER stress transducers in the unfolded-protein response. Nat. Cell Biol 2, 326–332 (2000). [PubMed: 10854322]

12. Calfon M, Zeng H, Urano F, Till JH, Hubbard SR, Harding HP, Clark SG, Ron D, IRE1 couples endoplasmic reticulum load to secretory capacity by processing the XBP-1 mRNA. Nature 415, 92–96 (2002). [PubMed: 11780124]

13. Cox JS, Walter P, A novel mechanism for regulating activity of a transcription factor that controls the unfolded protein response. Cell 87, 391–404 (1996). [PubMed: 8898193]

14. Lee AH, Iwakoshi NN, Glimcher LH, XBP-1 regulates a subset of endoplasmic reticulum resident chaperone genes in the unfolded protein response. Mol. Cell. Biol 23, 7448–7459 (2003). [PubMed: 14559994]

15. Yamamoto K, Suzuki N, Wada T, Okada T, Yoshida H,Kaufman RJ, Mori K, Human HRD1 promoter carries a functional unfolded protein response element to which XBP1 but not ATF6 directly binds. J. Biochem 144, 477–486 (2008). [PubMed: 18664523]

16. Yoshida H, Matsui T, Hosokawa N, Kaufman RJ, Nagata K, Mori K, A time-dependent phase shift in the mammalian unfolded protein response. Dev. Cell 4, 265–271 (2003). [PubMed: 12586069]

17. Lee AH, Scapa EF, Cohen DE, Glimcher LH, Regulation of hepatic lipogenesis by the transcription factor XBP1. Science 320, 1492–1496 (2008). [PubMed: 18556558]

18. Fink EE, Moparthy S, Bagati A, Bianchi-Smiraglia A, Lipchick BC, Wolff DW, Roll MV, Wang J, Liu S, Bakin AV, Kandel ES, Lee AH, Nikiforov MA, XBP1-KLF9 axis acts as a molecular rheostat to control the transition from adaptive to cytotoxic unfolded protein response. Cell Rep. 25, 212–223.e4 (2018). [PubMed: 30282030]

19. Zhou Y, Lee J, Reno CM, Sun C, Park SW, Chung J, Lee J, Fisher SJ, White MF, Biddinger SB, Ozcan U, Regulation of glucose homeostasis through a XBP-1-FoxO1 interaction. Nat. Med 17, 356–365 (2011). [PubMed: 21317886]

20. Bettigole SE, Glimcher LH, Endoplasmic reticulum stress in immunity. Annu. Rev. Immunol 33, 107–138 (2015). [PubMed: 25493331]

21. Song M, Sandoval TA, Chae CS, Chopra S, Tan C, Rutkowski MR, Raundhal M, Chaurio RA, Payne KK, Konrad C, Bettigole SE, Shin HR, Crowley MJP, Cerliani JP, Kossenkov AV, Motorykin I, Zhang S, Manfredi G, Zamarin D, Holcomb K, Rodriguez PC, Rabinovich GA, Conejo-Garcia JR, Glimcher LH, Cubillos-Ruiz JR, IRE1α–XBP1 controls T cell function in ovarian cancer by regulating mitochondrial activity. Nature 562, 423–428 (2018). [PubMed: 30305738]

22. Cubillos-Ruiz JR, Silberman PC, Rutkowski MR, Chopra S, Perales-Puchalt A, Song M, Zhang S, Bettigole SE, Gupta D, Holcomb K, Ellenson LH, Caputo T, Lee AH, Conejo-Garcia JR, Glimcher LH, ER stress sensor XBP1 controls anti-tumor immunity by disrupting dendritic cell homeostasis. Cell 161, 1527–1538 (2015). [PubMed: 26073941]

23. Reimold AM, Iwakoshi NN, Manis J, Vallabhajosyula P, Szomolanyi-Tsuda E, Gravallese EM, Friend D, Grusby MJ, Alt F, Glimcher LH, Plasma cell differentiation requires the transcription factor XBP-1. Nature 412, 300–307 (2001). [PubMed: 11460154]

24. Bettigole SE, Lis R, Adoro S, Lee AH, Spencer LA, Weller PF, Glimcher LH, The transcription factor XBP1 is selectively required for eosinophil differentiation. Nat. Immunol 16, 829–837 (2015). [PubMed: 26147683]

25. Sha H, Yang L, Liu M, Xia S, Liu Y, Liu F, Kersten S, Qi L, Adipocyte spliced form of X-box-binding protein 1 promotes adiponectin multimerization and systemic glucose homeostasis. Diabetes 63, 867–879 (2014). [PubMed: 24241534]

26. Wang Y, Zhang Y, Yi P, Dong W, Nalin AP, Zhang J, Zhu Z, Chen L, Benson DM, Mundy-Bosse BL, Freud AG, Caligiuri MA, Yu J, The IL-15-AKT-XBP1s signaling pathway contributes to effector functions and survival in human NK cells. Nat. Immunol 20, 10–17 (2019). [PubMed: 30538328]

27. Dong H, Adams NM, Xu Y, Cao J, Allan DSJ, Carlyle JR, Chen X, Sun JC, Glimcher LH, The IRE1 endoplasmic reticulum stress sensor activates natural killer cell immunity in part by regulating c-Myc. Nat. Immunol 20, 865–878 (2019). [PubMed: 31086333]

28. Liu J, Ibi D, Taniguchi K, Lee J, Herrema H, Akosman B, Mucka P, Salazar Hernandez MA, Uyar MF, Park SW, Karin M, Ozcan U, Inflammation improves glucose homeostasis through IKKβ-XBP1s interaction. Cell 167, 1052–1066.e18 (2016). [PubMed: 27814504]

29. Lee J, Sun C, Zhou Y, Lee J, Gokalp D, Herrema H, Park SW, Davis RJ, Ozcan U, p38 MAPK-mediated regulation of Xbp1s is crucial for glucose homeostasis. Nat. Med 17, 1251–1260 (2011). [PubMed: 21892182]
30. Kaser A, Lee AH, Franke A, Glickman JN, Zeissig S, Tilg H, Nieuwenhuis EE, Higgins DE, Schreiber S, Glimcher LH, Blumberg RS, XBP1 links ER stress to intestinal inflammation and confers genetic risk for human inflammatory bowel disease. Cell 134, 743–756 (2008). [PubMed: 18775308]
31. Narni-Mancinelli E, Chaix J, Fenis A, Kerdiles YM, Yessaad N, Reynders A, Gregoire C, Luche H, Ugolini S, Tomasello E, Walzer T, Vivier E, Fate mapping analysis of lymphoid cells expressing the NKp46 cell surface receptor. Proc. Natl. Acad. Sci. U.S.A 108, 18324–18329 (2011). [PubMed: 22021440]
32. Fehniger TA, Suzuki K, Ponnappan A, VanDeusen JB, Cooper MA, Florea SM, Freud AG, Robinson ML, Durbin J, Caligiuri MA, Fatal leukemia in interleukin 15 transgenic mice follows early expansions in natural killer and memory phenotype $CD8^+$ T cells. J. Exp. Med 193, 219–232 (2001). [PubMed: 11208862]
33. Ma S, Yan J, Barr T, Zhang J, Chen Z, Wang LS, Sun JC, Chen J, Caligiuri MA, Yu J, The RNA m6A reader YTHDF2 controls NK cell antitumor and antiviral immunity. J. Exp. Med 218, (2021).
34. Chen X, Cubillos-Ruiz JR, Endoplasmic reticulum stress signals in the tumour and its microenvironment. Nat. Rev. Cancer 21, 71–88 (2021). [PubMed: 33214692]
35. Getts MT, Getts DR, Kohm AP, Miller SD, Endoplasmic reticulum stress response as a potential therapeutic target in multiple sclerosis. Therapy 5, 631–640 (2008). [PubMed: 20357912]
36. Stone S, Lin W, The unfolded protein response in multiple sclerosis. Front. Neurosci 9, 264 (2015). [PubMed: 26283904]
37. Poggi A, Massaro AM, Negrini S, Contini P, Zocchi MR, Tumor-induced apoptosis of human IL-2-activated NK cells: Role of natural cytotoxicity receptors. J. Immunol 174, 2653–2660 (2005). [PubMed: 15728472]
38. Eischen CM, Schilling JD, Lynch DH, Krammer PH, Leibson PJ, Fc receptor-induced expression of Fas ligand on activated NK cells facilitates cell-mediated cytotoxicity and subsequent autocrine NK cell apoptosis. J. Immunol 156, 2693–2699 (1996). [PubMed: 8609385]
39. Screpanti V, Wallin RP, Ljunggren HG, Grandien A, A central role for death receptor-mediated apoptosis in the rejection of tumors by NK cells. J. Immunol 167, 2068–2073 (2001). [PubMed: 11489989]
40. Quinlan AR, Hall IM, BEDTools: A flexible suite of utilities for comparing genomic features. Bioinformatics 26, 841–842 (2010). [PubMed: 20110278]
41. Fox CJ, Hammerman PS, Cinalli RM, Master SR, Chodosh LA, Thompson CB, The serine/threonine kinase Pim-2 is a transcriptionally regulated apoptotic inhibitor. Genes Dev. 17, 1841–1854 (2003). [PubMed: 12869584]
42. Daenthanasanmak A, Wu Y, Iamsawat S, Nguyen HD, Bastian D, Zhang M, Sofi MH, Chatterjee S, Hill EG, Mehrotra S, Kraft AS, Yu XZ, PIM-2 protein kinase negatively regulates T cell responses in transplantation and tumor immunity. J. Clin. Invest 128, 2787–2801 (2018). [PubMed: 29781812]
43. Mikkers H, Nawijn M, Allen J, Brouwers C, Verhoeven E, Jonkers J, Berns A, Mice deficient for all PIM kinases display reduced body size and impaired responses to hematopoietic growth factors. Mol. Cell. Biol 24, 6104–6115 (2004). [PubMed: 15199164]
44. Lu J, Zavorotinskaya T, Dai Y, Niu XH, Castillo J, Sim J, Yu J, Wang Y, Langowski JL, Holash J, Shannon K, Garcia PD, Pim2 is required for maintaining multiple myeloma cell growth through modulating TSC2 phosphorylation. Blood 122, 1610–1620 (2013). [PubMed: 23818547]
45. Yan B, Zemskova M, Holder S, Chin V, Kraft A, Koskinen PJ, Lilly M, The PIM-2 kinase phosphorylates BAD on serine 112 and reverses BAD-induced cell death. J. Biol. Chem 278, 45358–45367 (2003). [PubMed: 12954615]
46. Zhang Y, Wang Z, Li X, Magnuson NS, Pim kinase-dependent inhibition of c-Myc degradation. Oncogene 27, 4809–4819 (2008). [PubMed: 18438430]

47. Peng C, Knebel A, Morrice NA, Li X, Barringer K, Li J, Jakes S, Werneburg B, Wang L, Pim kinase substrate identification and specificity. J. Biochem 141, 353–362 (2007). [PubMed: 17234686]
48. Gomez-Abad C, Pisonero H, Blanco-Aparicio C, Roncador G, Gonzalez-Menchen A, Martinez-Climent JA, Mata E, Rodriguez ME, Munoz-Gonzalez G, Sanchez-Beato M, Leal JF, Bischoff JR, Piris MA, PIM2 inhibition as a rational therapeutic approach in B-cell lymphoma. Blood 118, 5517–5527 (2011). [PubMed: 21937691]
49. Ren K, Gou X, Xiao M, Wang M, Liu C, Tang Z, He W, The over-expression of Pim-2 promote the tumorigenesis of prostatic carcinoma through phosphorylating eIF4B. Prostate 73, 1462–1469 (2013). [PubMed: 23813671]
50. Deng G, Nagai Y, Xiao Y, Li Z, Dai S, Ohtani T, Banham A, Li B, Wu SL, Hancock W, Samanta A, Zhang H, Greene MI, Pim-2 kinase influences regulatory T cell function and stability by mediating Foxp3 protein N-terminal phosphorylation. J. Biol. Chem 290, 20211–20220 (2015). [PubMed: 25987564]
51. An N, Lin YW, Mahajan S, Kellner JN, Wang Y, Li Z, Kraft AS, Kang Y, Pim1 serine/threonine kinase regulates the number and functions of murine hematopoietic stem cells. Stem Cells 31, 1202–1212 (2013). [PubMed: 23495171]
52. Lugo-Villarino G, Maldonado-Lopez R, Possemato R, Penaranda C, Glimcher LH, T-bet is required for optimal production of IFN-gamma and antigen-specific T cell activation by dendritic cells. Proc. Natl. Acad. Sci. U.S.A 100, 7749–7754 (2003). [PubMed: 12802010]
53. Townsend MJ, Weinmann AS, Matsuda JL, Salomon R, Farnham PJ, Biron CA, Gapin L, Glimcher LH, T-bet regulates the terminal maturation and homeostasis of NK and Valpha14i NKT cells. Immunity 20, 477–494 (2004). [PubMed: 15084276]
54. Yang Y, Ochando JC, Bromberg JS, Ding Y, Identification of a distant T-bet enhancer responsive to IL-12/Stat4 and IFNgamma/Stat1 signals. Blood 110, 2494–2500 (2007). [PubMed: 17575072]
55. Becknell B, Caligiuri MA, Interleukin-2, interleukin-15, and their roles in human natural killer cells. Adv. Immunol 86, 209–239 (2005). [PubMed: 15705423]
56. Yu J, Freud AG, Caligiuri MA, Location and cellular stages of natural killer cell development. Trends Immunol. 34, 573–582 (2013). [PubMed: 24055329]
57. Osorio F, Tavernier SJ, Hoffmann E, Saeys Y, Martens L, Vetters J, Delrue I, De Rycke R, Parthoens E, Pouliot P, Iwawaki T, Janssens S, Lambrecht BN, The unfolded-proteinresponse sensor IRE-1α regulates the function of CD8α$^+$ dendritic cells. Nat. Immunol 15, 248–257 (2014). [PubMed: 24441789]
58. Liu E, Marin D, Banerjee P, Macapinlac HA, Thompson P, Basar R, Nassif Kerbauy L, Overman B, Thall P, Kaplan M, Nandivada V, Kaur I, Nunez Cortes A, Cao K, Daher M, Hosing C, Cohen EN, Kebriaei P, Mehta R, Neelapu S, Nieto Y, Wang M, Wierda W, Keating M, Champlin R, Shpall EJ, Rezvani K, Use of CAR-transduced natural killer cells in CD19-positive lymphoid tumors. N. Engl. J. Med 382, 545–553 (2020). [PubMed: 32023374]
59. Miller SD, Karpus WJ, Experimental autoimmune encephalomyelitis in the mouse. Curr. Protoc. Immunol Chapter 15, 15.1.1–15.1.18 (2007).
60. Yu J, Wei M, Boyd Z, Lehmann EB, Trotta R, Mao H, Liu S, Becknell B, Jaung MS, Jarjoura D, Marcucci G, Wu LC, Caligiuri MA, Transcriptional control of humanT-BET expression: The role of Sp1. Eur. J. Immunol 37, 2549–2561 (2007). [PubMed: 17705132]
61. Fedele M, Pentimalli F, Baldassarre G, Battista S, Klein-Szanto AJ, Kenyon L, Visone R, De Martino I, Ciarmiello A, Arra C, Viglietto G, Croce CM, Fusco A, Transgenic mice overexpressing the wild-type form of the HMGA1 gene develop mixed growth hormone/prolactin cell pituitary adenomas and natural killer cell lymphomas. Oncogene 24, 3427–3435 (2005). [PubMed: 15735694]
62. Yu J, Wei M, Becknell B, Trotta R, Liu S, Boyd Z, Jaung MS, Blaser BW, Sun J, Benson DM Jr., Mao H, Yokohama A, Bhatt D, Shen L, Davuluri R, Weinstein M, Marcucci G, Caligiuri MA, Pro- and antiinflammatory cytokine signaling: Reciprocal antagonism regulates interferon-gamma production by human natural killer cells. Immunity 24, 575–590 (2006). [PubMed: 16713975]

63. Andrews S, FastQC: A quality control tool for high throughput sequence data, http://bioinformatics.babraham.ac.uk/projects/fastqc/, Babraham Bioinforma, http://bioinformatics.babraham.ac.uk/projects/ (2010).

64. Langmead B, Salzberg SL, Fast gapped-read alignment with Bowtie 2. Nat. Methods 9, 357–359 (2012). [PubMed: 22388286]

65. Feng J, Liu T, Qin B, Zhang Y, Liu XS, Identifying ChIP-seq enrichment using MACS. Nat. Protoc 7, 1728–1740 (2012). [PubMed: 22936215]

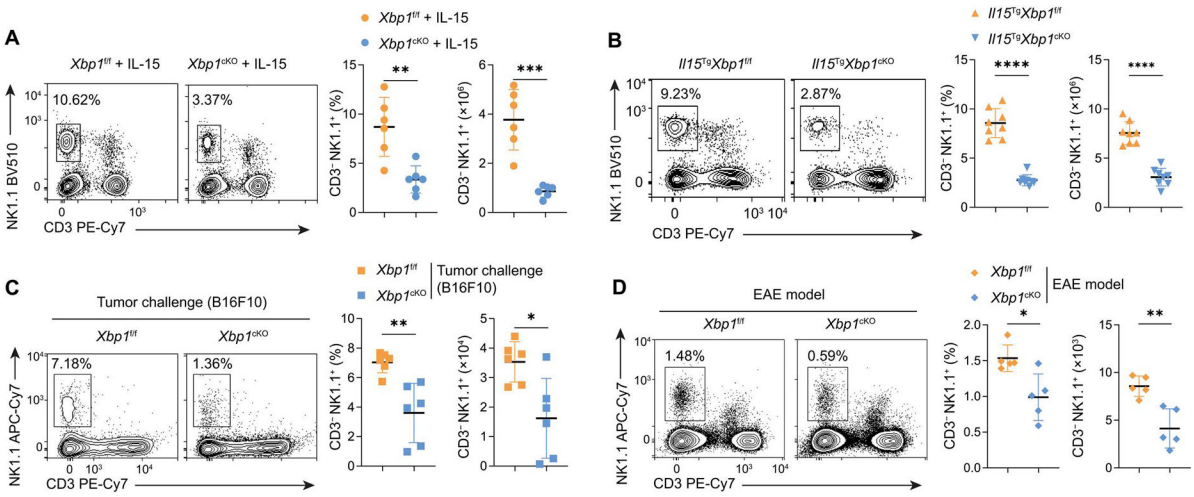

Fig. 1. XBP1s contributes to NK cell homeostasis in mice under ER stress.

(**A**) Representative plots (left) and summary data (right) of the percentages and absolute numbers of NK cells in the spleens from *Xbp1*$^{f/f}$ and *Xbp1*^{cKO} mice treated with IL-15 for 5 days ($n = 6$ per group). (**B**) Representative plots (left) and summary data (right) of the percentages and the absolute numbers of NK cells in the spleens from *Il15*^{Tg}*Xbp1*$^{f/f}$ and *Il15*^{Tg}*Xbp1*^{cKO} mice ($n = 8$ per group). (**C**) Representative plots (left) and summary data (right) of the percentages and the absolute numbers of NK cells in the lungs from B16F10 tumor-bearing *Xbp1*$^{f/f}$ and *Xbp1*^{cKO} mice ($n = 6$ per group). (**D**) Representative plots (left) and summary data (right) of the percentages and the absolute numbers of NK cells in the brains from *Xbp1*$^{f/f}$ and *Xbp1*^{cKO} mice at the onset of the EAE ($n = 5$ per group). Data are shown as means ± SD and were analyzed with an unpaired two-tailed *t* test. Data are representative of at least two independent experiments. *$P < 0.05$; **$P < 0.01$; ***$P < 0.001$; ****$P < 0.0001$.

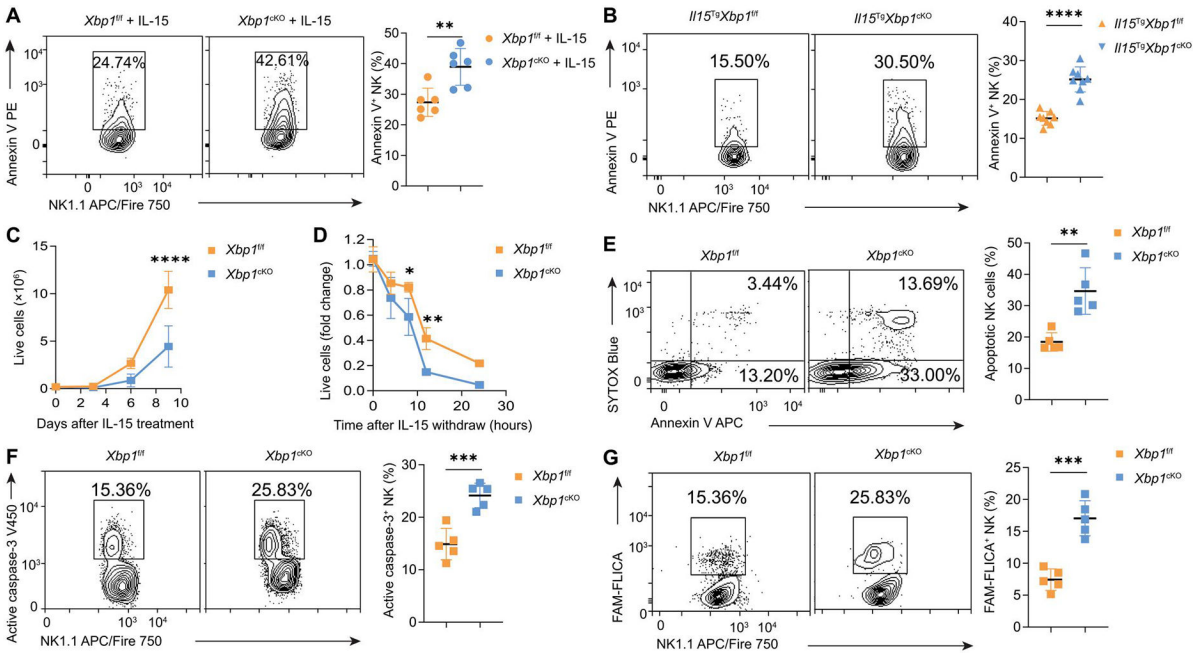

Fig. 2. XBP1s controls IL-15–mediated NK cell survival in vitro and in vivo.

(**A**) Percentages of annexin V$^+$ NK cells in the spleens from *Xbp1*$^{f/f}$ and *Xbp1*^{cKO} mice treated with IL-15 (n = 6 per group). (**B**) Percentages of annexin V$^+$ NK cells in the spleens from *Il15*^{Tg}*Xbp1*$^{f/f}$ and *Il15*^{Tg}*Xbp1*^{cKO} mice (n = 8 per group). (**C**) Splenic NK cells isolated from *Il15*^{Tg}*Xbp1*$^{f/f}$ and *Il15*^{Tg} *Xbp1*^{cKO} mice were cultured in vitro in the presence of IL-15 (50 ng/ml), followed by cell counting with a trypan blue exclusion assay. (**D**) Live NK cells were counted at 4, 8, 12, and 24 hours after IL-15 withdrawal. Data shown are the fold change from the data collected at 0 hours. (**E**) Representative plots (left) and summary data (right) of apoptotic (annexin V$^+$SYTOX Blue$^{+/-}$) NK cells from *Xbp1*$^{f/f}$ and *Xbp1*^{cKO} mice 5 days after in vitro culture with IL-15 (50 ng/ml). (**F**) Representative plots (left) and summary data (right) of apoptotic (active caspase-3$^+$) NK cells from *Xbp1*$^{f/f}$ and *Xbp1*^{cKO} mice 5 days after in vitro culture with IL-15 (50 ng/ml). (**G**) Representative plots (left) and summary data (right) of apoptotic (FAM-FLICA$^+$) NK cells from *Xbp1*$^{f/f}$ and *Xbp1*^{cKO} mice 5 days after in vitro culture with IL-15 (50 ng/ml). Data are shown as means ± SD and were analyzed with an unpaired two-tailed t test (A, B, and E to G) or two-way ANOVA with the Holm-Šídák post-test (C and D). Data are representative of at least two independent experiments. *P < 0.05; **P < 0.01; ***P < 0.001; ****P < 0.0001.

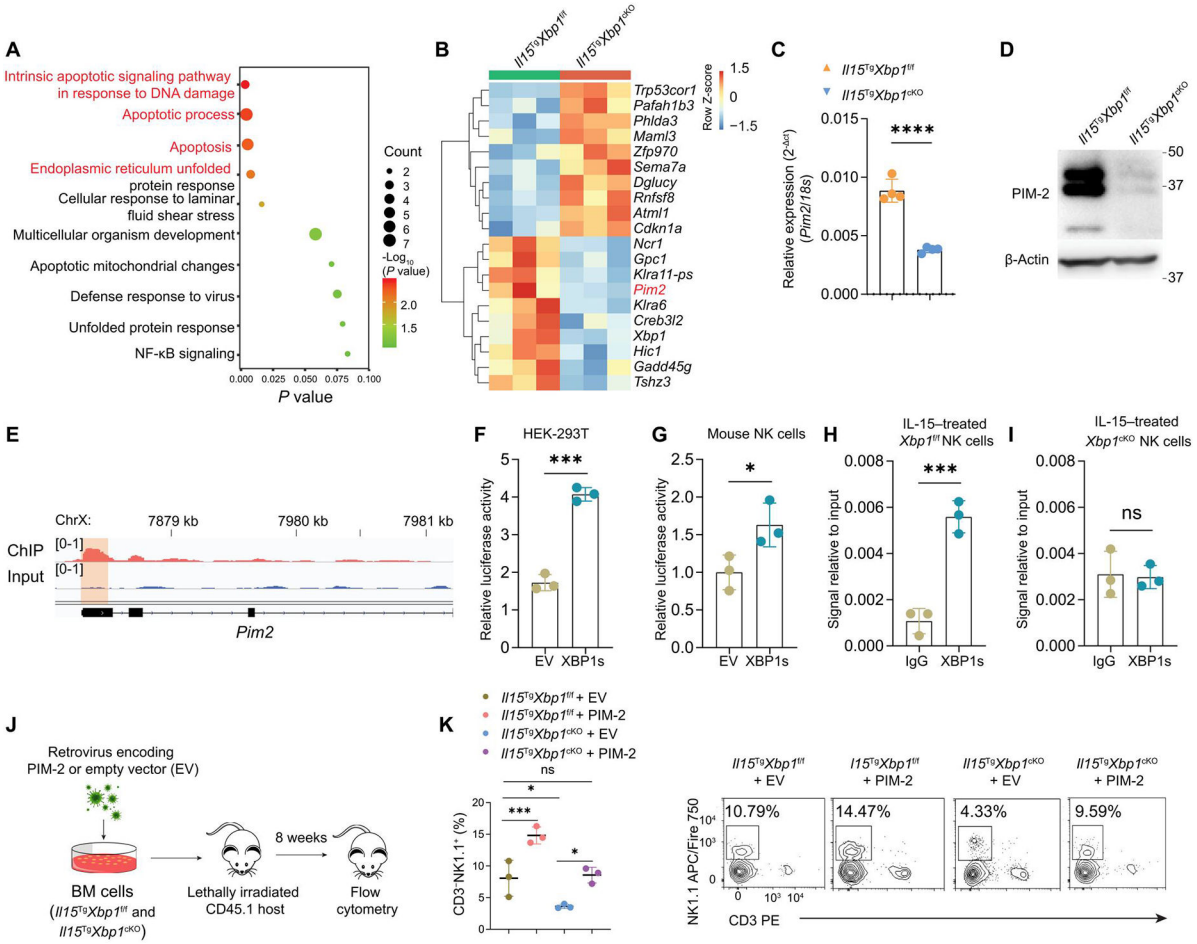

Fig. 3. XBP1s maintains NK cell survival by targeting PIM-2.

(**A**) Top 10 Gene Ontology clusters of DEGs in RNA-seq data. (**B**) Heat maps of top 20 genes expressed differentially between *Il15*^{Tg}*Xbp1*$^{f/f}$ and *Il15*^{Tg}*Xbp1*^{cKO} mice. (**C** and **D**) qPCR (C) and immunoblotting (D) showing expression levels of PIM-2 in NK cells from *Il15*^{Tg}*Xbp1*$^{f/f}$ and *Il15*^{Tg}*Xbp1*^{cKO} mice ($n = 4$ per group). (**E**) Integrative Genomics Viewer tracks displaying the distribution of XBP1s-binding peaks across the *Pim2* transcript. (**F** and **G**) Luciferase reporter assay showing that XBP1s activates *Pim2* gene transcription in HEK-293T cells (F) and mouse NK cells (G). (**H** and **I**) Binding of XBP1s to the *Pim2* promoter in IL-15–treated Xbp1$^{f/f}$ NK cells (H) or IL-15–treated *Xbp1*^{cKO} NK cells (I) was determined by ChIP-qPCR. (**J**) Scheme for retroviral transduction and BM chimeras. BM cells from *Il15*^{Tg}*Xbp1*$^{f/f}$ and *Il15*^{Tg}*Xbp1*^{cKO} mice were infected with retrovirus encoding *Pim2* or empty vector (EV). The infected cells were transferred into lethally irradiated CD45.1 recipient mice. After 8 weeks, mice were intraperitoneally injected with 2 μg of recombinant human IL-15 for 5 days. NK cells were isolated from the spleens of the chimeric mice and subjected to flow cytometry. (**K**) Summary data (left) and representative plots (right) of NK cells in chimeric mice ($n = 3$ per group). Data are shown as means ± SD and were analyzed with an unpaired two-tailed *t* test (C and F to I) or two-way ANOVA with the Holm-Šídák post-test (K). Data are representative of at least two independent experiments. ns, not significant; *$P < 0.05$; ***$P < 0.001$; ****$P < 0.0001$.

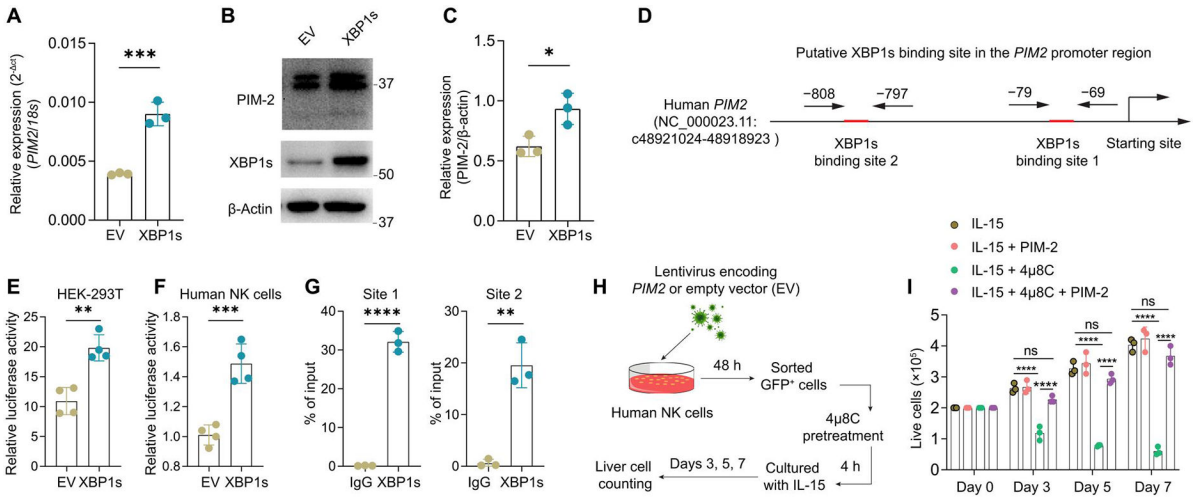

Fig. 4. XBP1s maintains cell survival by targeting PIM-2 in human NK cells.

(**A** to **C**) qPCR (A) and immunoblotting (B and C) showing PIM-2 levels in human NK cells transduced with XBP1s lentivirus ($n = 3$ per group). (**D**) Scheme denoting putative XBP1s-binding sites in the *PIM2* promoter. (**E** and **F**) Luciferase reporter assay showing that XBP1s activates *PIM2* gene transcription in HEK-293T cells (E) and human NK cells (F). (**G**) Binding of XBP1s to the *PIM2* promoter in human NK cells was determined by ChIP-qPCR. (**H** and **I**) Scheme for lentiviral transduction of PIM-2 into human NK cells and treatment with an inhibitor of IRE1α 4μ8C (50 μM) and IL-15 (50 ng/ml) (H). Live NK cell numbers were counted at the indicated time using a trypan blue exclusion assay [(I), $n = 3$ per group]. Data are shown as means ± SD and were analyzed with an unpaired two-tailed *t* test (A, C, and E to G) or one-way ANOVA with the Holm-Šídák post-test (I). Data are representative of at least two independent experiments. *$P < 0.05$; **$P < 0.01$; ***$P < 0.001$; ****$P < 0.0001$.

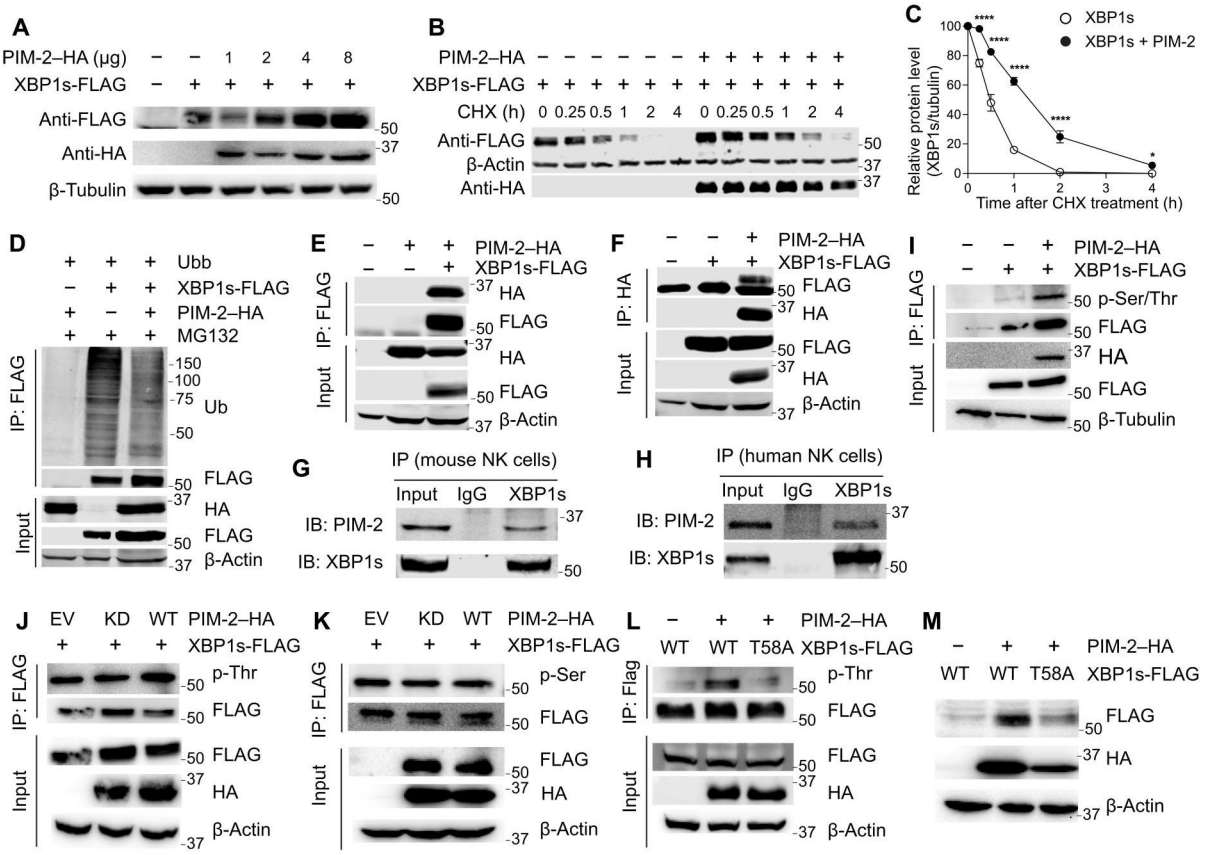

Fig. 5. PIM-2 stabilizes XBP1s protein through phosphorylation at Thr^{58}.

(**A**) FLAG-tagged XBP1s and different doses of HA-tagged PIM-2 were transiently transfected into HEK-293T cells. XBP1s levels were analyzed by immunoblotting. (**B** and **C**) HEK-293T cells were transiently transfected with FLAG-tagged XBP1s or together with HA-tagged PIM-2 and further treated with CHX for the indicated time periods. XBP1s levels were analyzed by immunoblotting. Representative blots (B) and quantification of immunoblotting signals of XBP1s to actin levels (C) are shown. (**D**) HEK-293T cells were transiently transfected with the FLAG-tagged XBP1s and Ubb plasmids with or without the HA-tagged PIM-2 plasmid. Ubiquitinylated XBP1s levels were analyzed by immunoblotting. (**E**) Immunoblotting for HA-tagged PIM-2 and FLAG-tagged XBP1s proteins after immunoprecipitation of FLAG from HEK-293T cells. (**F**) Immunoblotting for HA-tagged PIM-2 and FLAG-tagged XBP1s proteins after immunoprecipitation of HA from HEK-293T cells. (**G**) IL-2–expanded mouse NK cells were treated with IL-15 (50 ng/ml) for 24 hours. Cell lysates were immunoprecipitated with rabbit anti-XBP1s or IgG isotype control and immunoblotted with rabbit anti–PIM-2 or mouse anti-XBP1s. (**H**) Primary human NK cells were treated with IL-15 (50 ng/ml) for 24 hours. Cell lysates were immunoprecipitated with rabbit anti-XBP1s or IgG isotype control and immunoblotted with rabbit anti–PIM-2 or mouse anti-XBP1s. (I) Immunoblotting using a phospho-Thr/Ser–specific antibody to detect phosphorylated XBP1s levels after immunoprecipitation of FLAG from HEK-293T cells. (**J** and **K**) FLAG-tagged XBP1s and HA-tagged PIM-2 (WT or KD PIM-2, K61A) were transfected into HEK-293T cells. Immunoblotting using phospho-Thr–

specific (J) or phospho-Ser–specific antibody (K) for detecting phosphorylated XBP1s levels after immunoprecipitation of FLAG from HEK-293T cells. (**L**) FLAG-tagged WT XBP1s or Thr^{58} mutant (T58A) XBP1s and HA-tagged PIM-2 were transfected into HEK-293T cells. Immunoblotting using phospho-Thr–specific antibody to detect phosphorylated XBP1s levels after immunoprecipitation of FLAG from HEK-293T cells. (**M**) HEK-293T cells were transiently transfected with FLAG-tagged XBP1s or T58A mutant XBP1s together with HA-tagged PIM-2 and further treated with CHX for 1 hour. XBP1s levels were analyzed by immunoblotting. Data are shown as means ± SD and were analyzed with two-way ANOVA with the Holm-Šídák post-test (C). Data are representative of at least two independent experiments. $*P < 0.05$; $****P < 0.0001$.

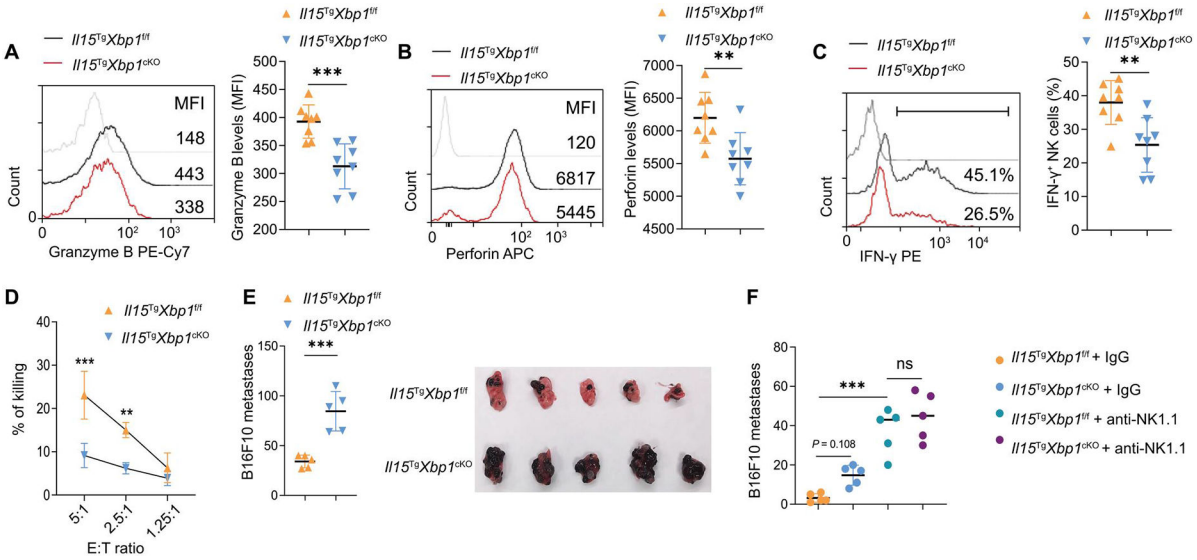

Fig. 6. XBP1s deficiency impairs NK cell effector functions and antitumor immunity.

(**A** to **C**) Expression levels of granzyme B (A), perforin (B), and IFN-γ (C) in NK cells from *Il15*^{Tg}*Xbp1*$^{f/f}$ and *Il15*^{Tg}*Xbp1*^{cKO} mice ($n = 8$ per group). (**D**) Poly(I:C)-activated NK cells were isolated from the spleen and cocultured with YAC-1 cells at a ratio of 5:1, 2.5:1, and 1.25:1 for 4 hours. Cytotoxicity of NK cells was evaluated by standard ^{51}Cr release assays ($n = 3$ per group). (**E**) *Il15*^{Tg}*Xbp1*$^{f/f}$ and *Il15*^{Tg}*Xbp1*^{cKO} mice were intravenously injected with B16F10 cells (2×10^5). Fourteen days after injection, mice were euthanized for postmortem analysis. Quantification of total metastatic nodules in the lung and the gross morphology of individual lung lobes are shown ($n = 5$ per group). (**F**) *Il15*^{Tg}*Xbp1*$^{f/f}$ and *Il15*^{Tg}*Xbp1*^{cKO} mice were intravenously injected with B16F10 cells (2×10^5) together with intraperitoneal injection of anti-NK1.1 antibody or IgG antibody (200 μg per mouse) on days 0 and 7 after tumor inoculation. The data show quantification of total metastatic nodules in the lung on day 14 ($n = 5$ per group). Data are shown as means ± SD and were analyzed with an unpaired two-tailed *t* test (A to E) or two-way ANOVA with the Holm-Šídák post-test (F). Data are representative of at least two independent experiments. $^{**}P < 0.01$; $^{***}P < 0.001$.

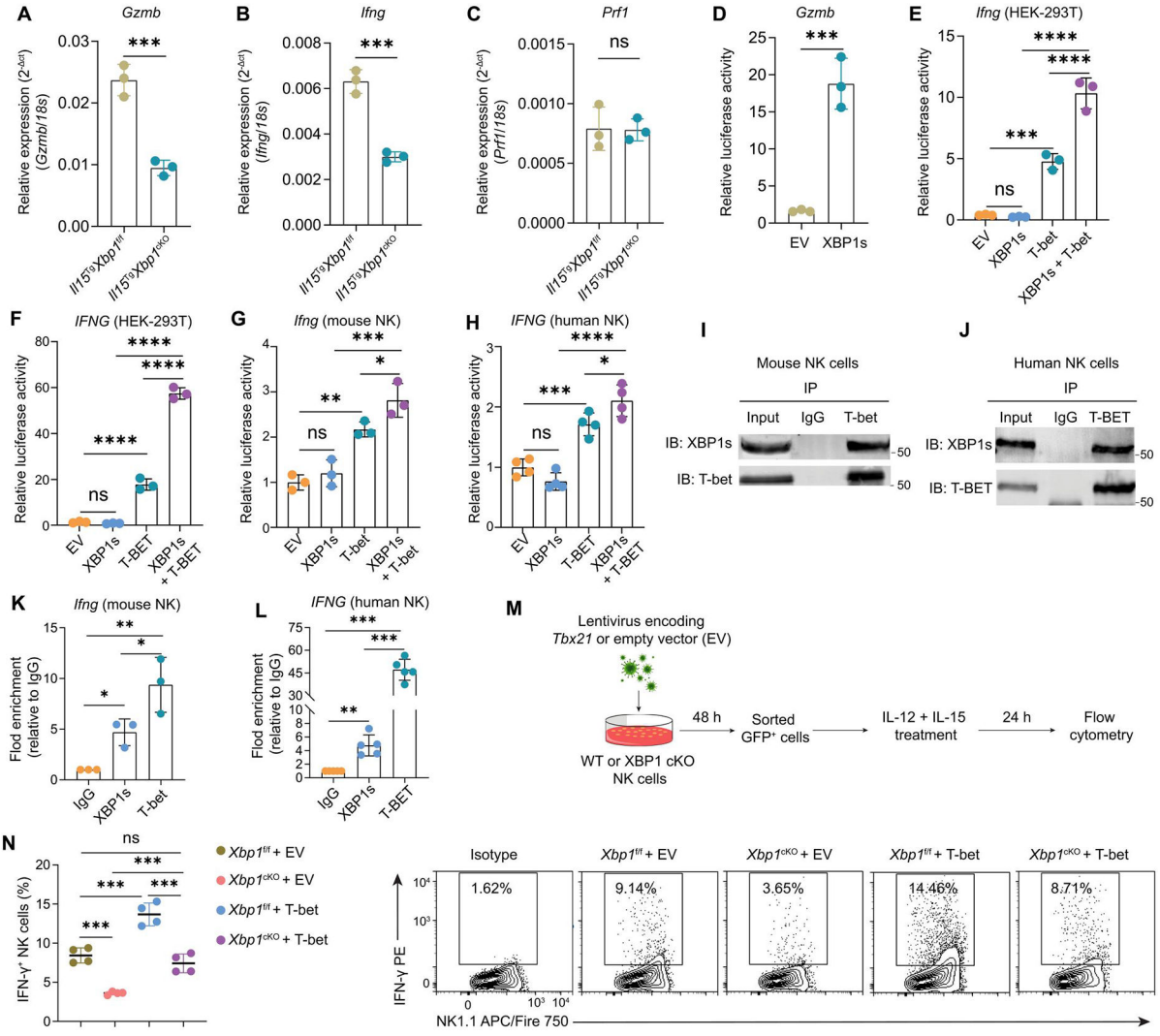

Fig. 7. XBP1s promotes IFN-γ production by recruiting T-bet to the promoter region of *Ifng*.

(**A** to **C**) qPCR analysis of mRNA levels of *Ifng* (A), *Gzmb* (B), and *Prf1* (C) in NK cells isolated from tumor tissues of *Il15*^{Tg}*Xbp1*$^{f/f}$ and *Il15*^{Tg}*Xbp1*^{cKO} tumor-bearing mice. (**D**) Luciferase reporter assay showing transcriptional activity of *Gzmb* after XBP1s overexpression. (**E**) Mouse XBP1s and T-bet were transfected alone or together into HEK-293T cells. The transcriptional activity of *Ifng* was examined by luciferase reporter assays. (**F**) Human XBP1s and T-BET were transfected alone or together into HEK-293T cells. The transcriptional activity of *IFNG* was examined by luciferase reporter assays. (**G**) Mouse XBP1s and T-bet were transfected alone or together into mouse NK cells. The transcriptional activity of *Ifng* was examined by luciferase reporter assays. (**H**) Human XBP1s and T-BET were transfected alone or together into human NK cells. The transcriptional activity of *IFNG* was examined by luciferase reporter assays. (**I**) IL-2–expanded mouse NK cells were treated with IL-15 (50 ng/ml) for 24 hours. Cell lysates were immunoprecipitated with rabbit anti–T-bet or IgG isotype control and immunoblotted with mouse anti-XBP1s or rabbit anti–T-bet. (**J**) Primary human NK cells were treated with IL-15 (50 ng/ml) for 24 hours. Cell lysates were immunoprecipitated with rabbit

anti–T-bet or IgG isotype control and immunoblotted with mouse anti-XBP1s or rabbit anti–T-bet. (**K**) The cross-linked DNA-protein complexes in IL-15–activated mouse NK cells were separately immunoprecipitated using antibodies against XBP1s or T-bet. The binding of XBP1/T-bet complex to the *Ifng* promoter was determined by ChIP-qPCR. (**L**) The cross-linked DNA-protein complexes in IL-15–activated human NK cells were separately immunoprecipitated using antibodies against XBP1s or T-BET. The binding of XBP1/T-BET complex to the *IFNG* promoter was determined by ChIP-qPCR. (**M** and **N**) Scheme for lentiviral transduction of T-bet into mouse NK cells (M). Data shown are summary data (left) and representative plots (right) that came from quantifying IFN-γ production by transduced NK cells [(N), $n = 4$ per group]. Data are shown as means ± SD and were analyzed with an unpaired two-tailed *t* test (A to D) or one-way ANOVA with the Holm-Šídák post-test (E to H, K, and L) or two-way ANOVA with the Holm-Šídák post-test (N). Data are representative of at least two independent experiments. $*P < 0.05$; $**P < 0.01$; $***P < 0.001$; $****p < 0.0001$.